AGU PUBLICATIONS

JGR

Journal of Geophysical Research: Atmospheres

RESEARCH ARTICLE
10.1002/2015JD024179

Key Points:
- Realistic seasonal mean values of lightning NO_x (LNO_x) production can be obtained from OMI data
- Mean LNO_x production over the Gulf of Mexico for five summers is 80 ± 45 mol per flash when adjusted for biases and uncertainties
- Biases and uncertainties in LNO_x estimates stemming from OMI data, elements of the algorithm, and flash data are quantified

Correspondence to:
K. E. Pickering,
Kenneth.E.Pickering@nasa.gov

Citation:
Pickering, K. E., E. Bucsela, D. Allen, A. Ring, R. Holzworth, and N. Krotkov (2016), Estimates of lightning NO_x production based on OMI NO_2 observations over the Gulf of Mexico, *J. Geophys. Res. Atmos.*, *121*, 8668–8691, doi:10.1002/2015JD024179.

Received 3 SEP 2015
Accepted 1 JUL 2016
Accepted article online 4 JUL 2016
Published online 19 JUL 2016

Estimates of lightning NO_x production based on OMI NO_2 observations over the Gulf of Mexico

Kenneth E. Pickering[1], Eric Bucsela[2], Dale Allen[3], Allison Ring[3], Robert Holzworth[4], and Nickolay Krotkov[1]

[1]Atmospheric Chemistry and Dynamics Laboratory, NASA Goddard Space Flight Center, Greenbelt, Maryland, USA, [2]SRI International, Menlo Park, California, USA, [3]Department of Atmospheric and Oceanic Science, University of Maryland, College Park, Maryland, USA, [4]Department of Earth and Space Sciences, University of Washington, Seattle, Washington, USA

Abstract We evaluate nitrogen oxide ($NO_x = NO + NO_2$) production from lightning over the Gulf of Mexico region using data from the Ozone Monitoring Instrument (OMI) aboard NASA's Aura satellite along with detection efficiency-adjusted lightning data from the World Wide Lightning Location Network (WWLLN). A special algorithm was developed to retrieve the lightning NO_x (LNO_x) signal from OMI. The algorithm in its general form takes the total slant column NO_2 from OMI and removes the stratospheric contribution and tropospheric background and includes an air mass factor appropriate for the profile of lightning NO_x to convert the slant column LNO_2 to a vertical column of LNO_x. WWLLN flashes are totaled over a period of 3 h prior to OMI overpass, which is the time an air parcel is expected to remain in a $1° \times 1°$ grid box. The analysis is conducted for grid cells containing flash counts greater than a threshold value of 3000 flashes that yields an expected LNO_x signal greater than the background. Pixels with cloud radiance fraction greater than a criterion value (0.9) indicative of highly reflective clouds are used. Results for the summer seasons during 2007–2011 yield mean LNO_x production of ~80 ± 45 mol per flash over the region for the two analysis methods after accounting for biases and uncertainties in the estimation method. These results are consistent with literature estimates and more robust than many prior estimates due to the large number of storms considered but are sensitive to several substantial sources of uncertainty.

1. Introduction

Global emissions of nitrogen oxides, known together as NO_x, are dominated by anthropogenic sources such as motor vehicles, electricity generation, and commercial and residential fossil fuel combustion. In the lower troposphere, air quality effects of NO_x emissions are most notable through their reactive contribution to tropospheric ozone (O_3) formation. Exposure to high O_3 mixing ratios can contribute to negative health consequences including lung-related illnesses such as asthma, especially for people in high-risk age groups. In the lower troposphere, the dominant form of NO_x is NO_2 because the NO reaction with ozone occurs at a faster rate than NO_2 conversion back to NO through photolysis. NO_2 reacts with the hydroxyl radical (OH), the primary oxidizing species in the atmosphere, to produce nitric acid (HNO_3), which is then wet or dry deposited [*Seinfeld and Pandis*, 2006; *Schumann and Huntrieser*, 2007]. This results in a NO_x lifetime of approximately 1 to 2 days in the lower troposphere [*Seinfeld and Pandis*, 2006] with an even shorter lifetime within the boundary layer.

While approximate source strengths for anthropogenically produced NO_x are known, considerable uncertainty exists for naturally produced NO_x [*Zhang et al.*, 2003; *Schumann and Huntrieser*, 2007]. Lightning is the largest natural source of NO_x, produced from splitting N_2 and O_2 diatomic molecules as a result of the extreme heat from lightning, forming NO in a process commonly referred to as the Zel'dovich Mechanism [*Zeldovich et al.*, 1947]. Lightning activity occurs primarily in the middle and upper troposphere. In the upper troposphere, NO_x has a lifetime on the order of several days [*Jaeglé et al.*, 1998; *Martin et al.*, 2007], because temperatures are colder and reaction rates are slowed [*Seinfeld and Pandis*, 2006]. At this altitude, NO_x can experience long-range transport, and O_3 production is more efficient in the upper troposphere than in the lower troposphere [*Pickering et al.*, 1990, 1996; *DeCaria et al.*, 2005; *Ott et al.*, 2007]. Other important precursors to tropospheric O_3 are the hydroxyl radical (OH) and the hydroperoxyl radical (HO_2) known together as HO_x. In the upper troposphere, HO_x is enhanced due to lightning NO production [*Labrador et al.*, 2004] and also due to the convective transport of HO_x precursors such as peroxides and formaldehyde. A maximum in

HO_x concentrations due to convection contributes to a peak in O_3 production on a short time scale (~4 h) over and immediately downwind of active convection [*DeCaria et al*., 2005]. However, enhanced ozone production continues well downwind of deep convective events.

Lightning contributes approximately 70% of the total NO_x concentration in the subtropical and tropical free troposphere [*Bond et al*., 2002; *Tie et al*., 2002; *Schumann and Huntrieser*, 2007; *Allen et al*., 2010]. LNO_x has been shown to enhance O_3 production several days downwind of active convection, in part due to the longer lifetime of NO_x in the upper troposphere [*Pickering et al*., 1993, 1996]. Clear skies downwind from active convection result in strong photolysis of NO_2, enhancing O_3 production especially between 500 and 300 hPa [*Labrador et al*., 2005]. *DeCaria et al*. [2005] found a maximum O_3 increase of 10–13 ppb downwind of midlatitude active convection at 10.5 km. *Hauglustaine et al*. [2001] found similar O_3 enhancements of 10–20 ppbv using global model simulations with and without LNO_x contributions. Globally, based on simulations with the NASA Global Modeling Initiative (GMI) model (see section 3.3), an estimated 60–70% of upper tropospheric NO_x and 35–45% of upper tropospheric O_3 has a lightning source [*Allen et al*., 2010]. Over the tropics these annual average percentages equal 70–80% and 45–55%. An estimated 60–90% of upper tropospheric NO_x concentrations and 15–35% of upper tropospheric O_3 concentrations over the United States during June, July, and August come from lightning NO [*Allen et al*., 2012]. The contribution varies regionally; however, the atmospheric modeling community is in agreement that upper tropospheric NO_x concentrations predominantly derive from lightning flashes in the tropics and summertime midlatitudes and that a significant portion of upper tropospheric O_3 production is attributable to LNO_x production. Therefore, a better understanding of the LNO_x source strength in tropical regions and midlatitude summer months where lightning flash rates are high is required.

In a changing climate, it is critical to develop a stronger understanding of the LNO_x contribution to middle and upper tropospheric O_3 production because O_3 is considered the third most important greenhouse gas [*Intergovernmental Panel on Climate Change*, 2013]. The ability of climate models to capture the contributions of LNO_x to O_3 production is needed for accurate climate prediction. *Liaskos et al*. [2015] evaluate the effects of the uncertainty in global lightning NO_x (LNO_x) production on upper tropospheric chemistry of NO_x, O_3, and OH using a global chemistry and climate model. For a factor of 4 increase in global LNO_x production (2.5 to 10 Tg N yr^{-1}), tropical upper tropospheric O_3 increases by up to 60%, yielding a factor of 3 increase in the mean net radiative flux due to O_3 at the tropopause.

In this study we use NO_2 column data from the Ozone Monitoring Instrument (OMI) on board NASA's Aura satellite, focusing on the Gulf of Mexico region, specifically between latitudes 23°N and 31°N and longitudes 78°W and 100°W. One of the earliest attempts at use of satellite NO_2 data [*Beirle et al*., 2006] for estimates of LNO_x production was conducted in this region. The region is well covered by several ground-based lightning detection networks and experiences minimal to moderate anthropogenic influence, an important consideration for choosing a study region because convective transport of boundary layer pollution may contribute to NO_x within thunderstorm anvils. To estimate the source strength of LNO_x per flash, the flash rate and total LNO_x production are required. To determine the flash rate, we use the World Wide Lightning Location Network (WWLLN) [*Dowden et al*., 2002; *Lay et al*., 2005; *Virts et al*., 2013], a ground-based detection network managed at the University of Washington. A global lightning climatology [*Cecil et al*., 2014] based on data from two satellite-based instruments, the Optical Transient Detector (OTD) in use between 1995 and 2000 [*Christian et al*., 2003; *Boccippio et al*., 2000] and the Lightning Imaging Sensor (LIS) operating from 1997 to 2015 [*Christian et al*., 1999, 2003; *Boccippio et al*., 2002; *Mach et al*., 2007], is used to estimate the WWLLN detection efficiency (DE). The OTD instrument recorded flashes from 70°N to 70°S latitude. LIS [*Christian et al*., 2003; *Boccippio et al*., 2002] flew aboard the Tropical Rainfall Measurement Mission (TRMM) satellite and sampled a particular field of view (600 × 600 km) for approximately 90 s [*Christian et al*., 1999; *Cecil et al*., 2014] each day over the latitude range 35°N to 35°S. The flash detection efficiency of LIS ranged from 68% at noon to 88% at night [*Christian et al*., 1999; *Boccippio et al*., 2002]. Due to its space-based platform, LIS could not distinguish between intracloud (IC) and cloud-to-ground (CG) flashes [*Christian et al*., 1999].

Due to the existence of ground-based and satellite-based lightning detection data, the mean regionally averaged lightning flash rate is relatively well understood. Therefore, the main reason for the uncertainty in representing LNO_x emissions in chemistry and climate models is the uncertainty surrounding the number of moles of LNO_x produced per flash (see Table 1 and section 2). Other reasons for the LNO_x emissions

Table 1. Compilation of Literature Estimates of Lightning-Generated NO Moles per Flash

Method	Moles NO/Flash (Notes)	Reference
Theoretical	1100 (CG), 110 (IC)	*Price et al.* [1997]
Laboratory	~103	*Wang et al.* [1998]
LMA/theoretical	604 (CG), 38 (IC)	*Koshak* [2014]
Aircraft data, cloud model	345–460 (STERAO-A)	*DeCaria et al.* [2005]
Aircraft data, cloud model	360 (STERAO-A, EULINOX)	*Ott et al.* [2007, 2010]
Aircraft data, cloud model	590–700 (CRYSTAL-FACE)	*Ott et al.* [2010]
	500 (mean midlatitude)	*Ott et al.* [2010]
Aircraft data, cloud model	500–600 (SCOUT-O3/ACTIVE)	*Cummings et al.* [2013]
Aircraft data	55–382 (CRYSTAL-FACE)	*Ridley et al.* [2004]
Aircraft data	70–210 (TROCCINOX)	*Huntrieser et al.* [2008]
Aircraft data	121–385 (SCOUT-O3/ACTIVE)	*Huntrieser et al.* [2009]
Aircraft data	70–179 (AMMA)	*Huntrieser et al.* [2011]
Satellite (GOME)	32–240 (subtropical)	*Beirle et al.* [2006]
Satellite (SCIAMACHY)	33–50 (global, mostly marine)	*Beirle et al.* [2010]
Satellite (OMI)	87–246 (TC4—tropical marine)	*Bucsela et al.* [2010]
	174 (TC4 mean)	*Bucsela et al.* [2010]

uncertainty include spatial biases in convective precipitation and in the relationship between convective parameters and flash rates [*Pickering et al.*, 1998; *Allen and Pickering*, 2002; *Tost et al.*, 2007; *Allen et al.*, 2010], as such variables are used to determine the number of flashes and their placement in the model domain.

In this study we will focus on estimation of the LNO_x production per flash in an effort to reduce the uncertainty in the global LNO_x emissions. To do this, we use a processing algorithm to estimate the column LNO_x from the OMI NO_2 data. In this algorithm, we use simulated LNO and LNO_2 profiles to convert the OMI tropospheric LNO_2 columns to LNO_x. We then examine the flashes coincident with the OMI LNO_x over a time interval prior to OMI overpass to generate an estimated average moles of LNO_x produced per flash for the subtropical Gulf of Mexico region. We first examine in detail the LNO_x production per flash in two particular seasons, June, July, and August (JJA) 2008 and JJA 2011, and then expand the analysis to include this season for all five years from 2007 to 2011.

Section 2 provides information on previous estimates of LNO_x production per flash. Section 3 describes the various data sets that are used in the analysis and discusses the methods that are employed. Section 4 describes the results of the analysis first for two specific seasons and then for the summers of five years, as well as the sources of uncertainty of our results. Section 5 discusses our results in comparison with previous studies, and section 6 summarizes the conclusions of our analysis.

2. Previous Estimates of Lightning NO_x Production

Current literature estimates of NO production per flash vary considerably for lightning events in tropical and midlatitude regimes as presented in Table 1 [see also *Schumann and Huntrieser*, 2007]. These estimates have been generated from theoretical analyses, model studies, in situ aircraft measurements during aircraft campaigns, and from satellite observations. Note that most of the tropical estimates are smaller than those for midlatitudes. *Huntrieser et al.* [2008] have hypothesized that shorter flash length due to less vertical wind shear may be responsible for the smaller tropical production per flash. Contributing to the lightning NO_x (LNO_x) production uncertainty, cloud-to-ground (CG) and intracloud (IC) lightning strokes may produce different amounts of NO_x due to differences in their energy per stroke and path length [*Gallardo and Cooray*, 1996; *Price et al.*, 1997]. NASA's Global Modeling Initiative (GMI) chemical transport model assumes a midlatitude lightning flash NO mean production value of 500 mol and a tropical lightning flash NO mean production value of 250 mol [*Allen et al.*, 2010]. GMI and some other models do not distinguish between IC and CG flash production rates because cloud-resolving model simulations constrained by observed flash rates and anvil NO_x observations have suggested that in the mean NO_x production by an IC flash is roughly equivalent to that of a CG flash.

Theoretical estimates support significant difference between the IC and CG flash production of NO [*Price et al.*, 1997]. *Koshak et al.* [2014] presented results from an LNO_x production model using theoretical and laboratory findings along with lightning mapping array data that also support substantial differences. *Koshak* [2014]

extended this analysis using 9 years of North Alabama Lightning Mapping Array and National Lightning Detection Network data and obtained mean CG production of 604 mol per flash and mean IC production of 38 mol per flash. However, cloud/chemistry modeling-based studies constrained by anvil aircraft observations find a much smaller difference between the source strengths of IC and CG flashes [*DeCaria et al*., 2005; *Ott et al*., 2007, 2010; *Huntrieser et al*., 2011; *Cummings et al*., 2013].

As seen in Table 1, estimates range from 32 to 1100 mol of NO per flash. Many of the values in Table 1 are from studies of individual storm events, which are then extrapolated to global estimates. The table suggests that geographic location (the midlatitudes versus the tropics) of individual storms affects the LNO_x production per flash. Considering the large range in the NO production per flash estimates, *Schumann and Huntrieser* [2007] reached a conclusion that the best global estimate of LNO_x production lies in the range of 2–8 Tg N yr^{-1}, with a most likely estimate of 5 Tg N yr^{-1} (~250 mol per flash on average, assuming the OTD/LIS climatological value of 46 flashes per second globally [*Cecil et al*., 2014]). With this factor of 4 range, upper tropospheric chemistry modeling remains uncertain [e.g., *Liaskos et al*., 2015].

With the significant variation in NO production per flash values shown in Table 1, a comprehensive global source of information on the LNO_x source is needed. In this study we use a satellite-based analysis to estimate the NO production per flash over the Gulf of Mexico region as a preliminary step for planned global LNO_x production estimates. This approach will allow us to examine tropical versus midlatitude regional variations in NO production per flash. It will also contribute to reduce the large range of uncertainty in the current estimates of NO production per flash used in global chemical transport models.

Recent studies have attempted to constrain the magnitude of the global LNO_x source using satellite observations of NO_2. However, accurate measurement from space of lightning-produced NO_x is difficult because anthropogenic sources are prolific and dominate total column satellite measurements. Satellite observations of LNO_x are challenging also because of complications due to cloud reflections and because most upper tropospheric NO_x exists in the form of NO, which is not directly detectable from space. However, *Beirle et al*. [2009] have demonstrated, through the use of cloud, chemistry, and radiative transfer modeling for a typical marine convective system, that nadir-viewing satellites likely have a good sensitivity to NO_2 inside a thunderstorm cloud, implying that LNO_2 should be well seen from space.

Beirle et al. [2004] used Global Ozone Monitoring Instrument (GOME) NO_2 column densities over Australia and LIS lightning data to estimate that lightning produces 2.8 Tg N yr^{-1}, but the range of uncertainty was large (0.8–14 Tg (N) yr^{-1}). *Beirle et al*. [2006] studied LNO_x production from a storm system in the Gulf of Mexico using GOME data and National Lightning Detection Network (NLDN) [*Cummins et al*., 1998] observations. Extrapolating their findings of 32–240 mol per flash to the global scale, they estimated an LNO_x source of 1.7 Tg N yr^{-1} with a range of uncertainty from 0.6 to 4.7 Tg (N) yr^{-1}. *Boersma et al*. [2005] used GOME NO_2 observations and the TM3 CTM with two different LNO_x parameterizations in global simulations and concluded that LNO_x production was between 1.1 and 6.4 Tg (N) yr^{-1}. *Martin et al*. [2007] used global GEOS-Chem simulations in conjunction with space-based observations of NO_2, ozone, and nitric acid to estimate LNO_x production of 6 ± 2 Tg (N) yr^{-1}. Their NO_2 data were obtained using the Scanning Imaging Absorption Spectrometer for Atmospheric Cartography/chemistry (SCIAMACHY) instrument.

Beirle et al. [2010] conducted a systematic analysis of LNO_x production using SCIAMACHY NO_2 observations (10 A.M. local time overpass) in conjunction with global flash observations from the World Wide Lightning Location Network (WWLLN). Only events with relatively high flash rates (after scaling for detection efficiency) in the hour prior to SCIAMACHY overpass were considered for analysis. Therefore, these events represent quite fresh LNO_x emissions from active storms. Although clear enhancements of NO_2 column densities were found in some cases, retrieved values were well below expected amounts, and in most cases no enhanced NO_2 was found. Due to the 10 A.M. observation time, the majority of the events studied were over the ocean. The largest values of production per flash (~200 mol per flash) were observed over the northern Gulf of Mexico and over the Atlantic east of Florida. Beirle et al. were uncertain whether these relatively large values are due to interference from convectively lofted pollution or to particularly productive flashes. There is evidence that oceanic CG flashes have larger peak currents than continental flashes [*Cooray et al*., 2014; *Chronis et al*., 2016] and that oceanic CG and IC flashes have greater "strength" [*Beirle et al*., 2014], which may explain the larger LNO_x production in these regions than over continents.

Bucsela et al. [2010] presented case studies identifying LNO_x observed during NASA's Tropical Composition, Cloud and Climate Coupling Experiment (TC^4) in July and August 2007. In the campaign, DC-8 aircraft missions, flown from Costa Rica, recorded in situ NO and NO_2 profiles near active storms and in relatively quiet areas. They combined these TC^4 DC-8 data with OMI data to estimate the lightning-generated NO_2 above background levels. Information on lightning flashes, primarily cloud-to-ground (CG), observed by the Costa Rica Lightning Detection Network and the WWLLN was examined over storms upwind of regions where OMI indicates enhanced LNO_2. These flash data were compared with LIS satellite data to estimate total flashes. Using $[NO_2]/[NO_x]$ ratios from NASA's GMI model, they estimated LNO_x production per flash for four cases and obtained rates of ~100–250 mol per flash. These are consistent with rates derived from previous studies (Table 1) of tropical and subtropical storms (mostly $<$250 mol per flash) and below those from modeling of observed midlatitude storms (mostly $>$300 mol per flash). In their study, environments with stronger anvil-level winds were associated with higher production rates and above-average LIS flash lengths. LNO_x enhancements over background determined from the OMI data were less than but roughly proportional to aircraft estimates. The algorithm used in the current paper (see section 3.4) is based on an approach similar to that used by *Bucsela et al*. [2010].

3. Data and Methods

3.1. Ozone Monitoring Instrument

The Dutch-Finnish Ozone Monitoring Instrument (OMI) is aboard the Aura spacecraft, a member of NASA's A-train Sun-synchronous polar orbiting satellite group. OMI detects a variety of molecules and aerosol characteristics and passes over the equator at 13:30 LT and over the Gulf of Mexico at ~13:45 LT. It has a 2600 km cross-track swath, with a binned ground pixel size at nadir of 13×24 km, increasing to a ground pixel size of 45×128 km at the outer edges of the swath [*Levelt et al*., 2006a, 2006b]. OMI uses a two-dimensional detector which allows for simultaneous retrievals across the field of view. It measures in the UV and visible range, between 270 and 500 nm, with the NO_2 signal derived from the visible range between 425 and 465 nm [*Levelt et al*., 2006a, 2006b]. We use level 2 processed data (OMNO2A), generated from a Differential Optical Absorption Spectroscopy algorithm, developed by the Royal Netherlands Meteorological Institute (KNMI), which yields a total slant column density (SCD) [*Boersma et al*., 2008] of NO_2. The standard processing of level 2 data at NASA Goddard to obtain NO_2 vertical column densities (VCDs) was significantly improved in version 2 from the previous version 1 processing algorithm because it improves cloud retrievals, the stratosphere-troposphere separation, and the temporal resolution (was annual and is now monthly) of a priori NO_2 profiles [*Bucsela et al*., 2013]. Due to an orbital "striping" effect [*Boersma et al*., 2011; *Bucsela et al*., 2013], the SCDs are destriped before standard level 2 VCDs are produced; a thorough discussion of the destriping algorithm is provided in *Bucsela et al*. [2013]. Using the level 2 processed NO_2 SCDs, we convert to LNO_x VCD using the offline dedicated algorithm described in section 3.4.

For the current study, we use daily NO_2 columns retrieved from OMI for the months of JJA 2008 and JJA 2011 over the Gulf of Mexico region. As of 25 June 2007, a row anomaly in the OMI data became evident, likely due to a partial obstruction of OMI's aperture [*Boersma et al*., 2011; *Bucsela et al*., 2013]. During JJA 2008, this minimally affected the OMI NO_2 data but in JJA 2011, the row anomaly was significant with only roughly 50% of the pixels available for use in scientific studies. This situation required a few days of data to be removed from our analysis due to inadequate sampling over the Gulf of Mexico. After discussing the results of these two seasons in detail, we present results for all summer months for 2007 through 2011.

3.2. World Wide Lightning Location Network

The LIS instrument on the TRMM satellite only recorded flashes over a given point on the Earth for about 90 s during an overpass. However, a continuous record of individual flashes is required for our OMI LNO_x analysis and that can only be obtained at present from a ground-based network. The World Wide Lightning Location Network (WWLLN) is a ground-based global network of stations that detect very low frequency (VLF) signals from lightning discharges called sferics within the 3–30 kHz range [*Dowden et al*., 2002; *Lay et al*., 2005; *Virts et al*., 2013]. WWLLN began recording reliable lightning data in 2004 and has increased its global coverage from 11 stations to about 70 stations today [*Lay et al*., 2004; *Hutchins et al*., 2013]. We use the WWLLN data in conjunction with OMI LNO_x retrievals to estimate the LNO_x production per flash for the Gulf of Mexico.

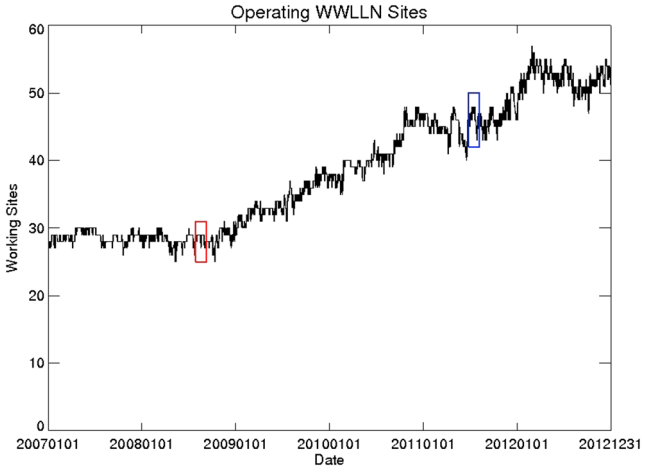

Figure 1. WWLLN stations operating each day between 1 January 2007 and 31 December 2012. August 2008 (red box) and July 2011 (blue box) are months used in the initial phase of this study.

Figure 1 shows that the number of working stations increased from approximately 28 in 2007 to approximately 55 in 2012. In August 2008, there were ~28 working stations, and in July 2011, there were ~43 working stations (see boxes in Figure 1). Some stations are in remote locations, and some are in countries troubled by political unrest making station continuity challenging. Intermittency of some stations can last days or months, negatively affecting the network detection efficiency.

A time of group arrival packet containing the stroke UTC date and time, stroke location, error in microseconds, and the number of stations that received the signal [*Rodger et al*., 2004, 2005] is recorded. Strong sferic discharges can travel significant distances (up to 10,000 km), especially over water, which is why a global network of less than 100 stations can be reliable for lightning stroke detection [*Lay et al*., 2005; *Rodger et al*., 2009]. In order for a stroke to be counted, a minimum of five WWLLN stations must detect a lightning signal [*Dowden et al*., 2002; *Rodger et al*., 2005]. Due to its detection frequency range (3–30 kHz), WWLLN is most efficient at detecting cloud to ground strokes but can detect some intracloud activity [*Rodger et al*., 2009; *Rudlosky and Shea*, 2013]. For a more detailed description of the WWLLN processing algorithm, please refer to the paper by *Rodger et al*. [2004].

Rudlosky and Shea [2013] computed the detection efficiency (DE) of WWLLN relative to LIS for the Western Hemisphere between 38°N and 38°S over the years 2009 to 2012 through matching of specific LIS flashes with WWLLN strokes. WWLLN relative DE was 15.2% over the ocean and 5.8% over land in 2011. In this study, we need monthly estimates of DE during the 2007 to 2012 time period for all 1° × 1° global grid boxes. To begin the DE calculation, the WWLLN stroke data are summed hourly on a 2° latitude × 2.5° longitude grid and then smoothed temporally and spatially via the applications of a running 31 day average, a 3 h average, and a 3 point north-south and east-west boxcar smoother. Next, for each grid box, the smoothed WWLLN strokes are summed for each of the sixty-one 12 month periods starting between January 2007 and January 2012 and compared to the v2.3 OTDLIS climatological flash rate at that grid box. The resulting ratios between the WWLLN sums and the OTDLIS sum provide an estimate of the DE for each of the sixty-one 12 month time periods. Monthly scaling factors are then obtained by averaging the annual scaling factors from the twelve 12 month time periods that contain the month of interest. These 12 month periods include 11 months before and after the month of interest. Therefore, the final monthly scaling factor for each grid box is a weighted average with the month of interest having a weighting of 12, the month before and after the month of interest having a weighting of 11, months 2 months away from the month of interest having a weighting of 10 and so forth. For example, scaling factors for July 2011 contain information from August 2010 to June 2012 with July 2011 having the most weight (12), June and August 2011 having a weighting of 11, and so forth until August 2010 and June 2012 have a weighting of one. The resulting month-specific DEs are then smoothed via the 3× application of a seven-point boxcar average and then interpolated onto the 1° × 1° global grid. Then the DEs at each grid box are adjusted to ensure that the DE-adjusted WWLLN flash rate on the 1° × 1° analysis grid over the 2007–2012 time period matches the OTDLIS climatological flash rate. Finally, an optional diel adjustment is applied to the DE-adjusted WWLLN flash rates. This step keeps the daily flash rate constant but constrains the diel variation in DE-adjusted WWLLN flash rates to better match the diel variation in version 2.3 of the OTD/LIS climatology. Figure 2 presents maps of the global distribution of WWLLN DE for August 2008 and July 2011 computed from the method described above and in *Allen et al*. [2014]. As the number of WWLLN stations increased from 2008 to 2011, the globally averaged (60°S–60°N) DE increases from 11 to 22% with the DE over the Gulf of Mexico region increasing from 11 to 31%.

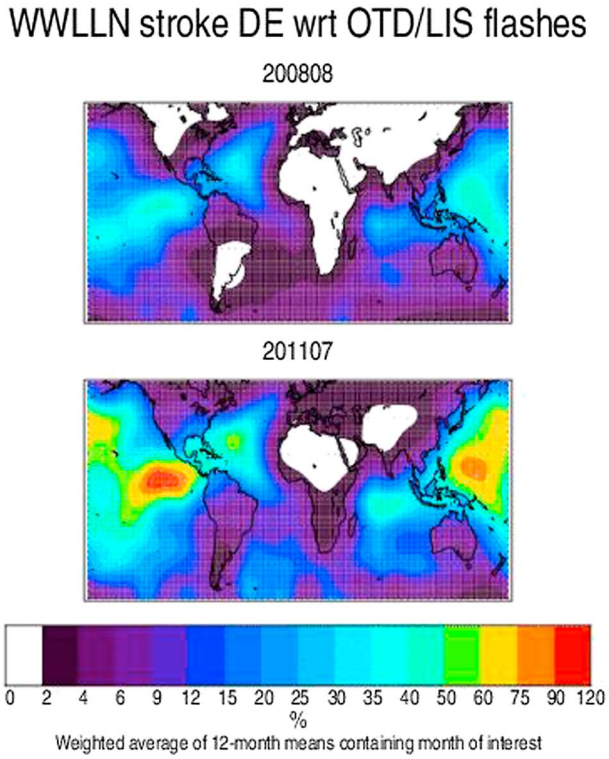

Figure 2. WWLLN stroke detection efficiency with respect to OTD/LIS flashes centered on (top) August 2008 and (bottom) July 2011.

3.3. Global Modeling Initiative—Chemical Transport Model

As described in section 3.4, monthly mean profiles of LNO_2 and LNO_x are needed as input to our LNO_x algorithm. We obtained profiles from the NASA Global Modeling Initiative (GMI) chemical transport model simulations that were performed with and without lightning. GMI is a NASA-supported coupled troposphere and stratosphere model [*Duncan et al.*, 2007; *Ziemke et al.*, 2006] that includes chemistry and transport, deposition, radiation, and aerosol microphysics [*Duncan et al.*, 2007]. More specifically, we used GMI Hindcast FF simulations [*Strode et al.*, 2015] which incorporate year-specific fossil fuel emissions based on EDGAR (Emission Database for Global Atmospheric Research) 2000 data with various regional inventories and scaling factors from GEOS-Chem (Goddard Earth Observing System-Chemical Transport Model) applied for other years [*van Donkelaar et al.*, 2008]. Hindcast FF simulations also use year-specific GFEDv3 (Global Fire Emissions Database v.3) biomass burning emissions [*van der Werf et al.*, 2010] with diurnal variation, Asian fossil fuel emissions from Intercontinental Chemical Transport Experiment (INTEX-B) inventories for 2006 [*Zhang et al.*, 2009] scaled to other years using GEOS-Chem scaling factors, and biofuels based on *Yevich and Logan* [2003] but overwritten with data from EPA/NEI99 over the United States. Lightning NO_x emissions are estimated based on *Allen et al.* [2010]. The GMI model is driven by GEOS-5 MERRA (Modern-Era Retrospective Analysis for Research and Applications) meteorological fields that have been regridded from 1° latitude × 1.25° longitude to 2° latitude × 2.5° longitude spatial resolution and a vertical grid of 72 pressure levels [*Rienecker et al.*, 2011].

A second set of simulations was executed from June 2006 to December 2012 without lightning NO_x emissions to provide ample spin-up time for our August 2008 and July 2011 analysis months. We extracted monthly NO and NO_2 profiles coincident with the OMI overpass time of 13:30 LT from both sets of simulations. Taking the difference of the vertical profiles between the standard Hindcast FF simulation and the simulation without lightning yields the LNO_x and LNO_2 vertical profiles used in the algorithm discussed in section 3.4. The magnitude of the vertical profiles is sensitive to the moles per flash assumptions used in the Hindcast FF simulations. However, this sensitivity has only minimal impact on the retrieval which is much more sensitive to the profile shape. Figure 3 shows monthly mean LNO_2 and LNO_x profiles over the Gulf of Mexico. Clearly, most LNO_x in the upper troposphere exists as NO adding to the difficulty of extracting a lightning NO_x signal from an OMI NO_2 retrieval. For application in the algorithm below the LNO_2 and LNO_x profiles from the day of the month with the fourth largest GMI LNO_x column amount in each GMI grid cell are used.

3.4. Algorithm

The full algorithm used to generate the LNO_x VCD is given by

$$V_{LNOx} = \frac{S_{Total} - V_{strat} \times AMF_{strat} - V_{BG} \times AMF_{trop}}{AMF_{LNOx}} \quad (1)$$

where S_{Total} is the OMI-measured NO_2 total SCD, V_{strat} is the OMI-retrieved stratospheric NO_2 VCD (Standard Product, version 2.1), and AMF_{strat} is the modeled stratospheric air mass factor used in the standard OMI product [*Bucsela et al*., 2013]. The VCD of stratospheric NO_2 for the specific day being analyzed is used in this algorithm. V_{BG} is the estimated tropospheric VCD due to all nonlightning NO_2 sources (i.e., "background"), which can be treated in multiple ways as discussed later in this section. AMF_{trop} is the modeled tropospheric air mass factor used in the standard OMI product [*Bucsela et al*., 2013], and AMF_{LNOx} is the air mass factor used to convert the SCD of LNO_2 to a VCD of LNO_x. It is computed by dividing the LNO_2 SCD that is modeled using radiative transfer and a profile of LNO_2 from the GMI model by an LNO_x VCD from the GMI model. For a thorough discussion of the AMF_{strat} and AMF_{trop} used in this analysis, please refer to the *Bucsela et al*. [2013] paper.

A minimum of five OMI pixels is required for producing a valid LNO_x amount for a grid cell such that noise is minimized. For each $1° \times 1°$ grid cell that satisfies the flash threshold and has at least five valid pixels, the vertical column LNO_x is obtained by averaging column LNO_x values from all OMI pixels in the cell. This mean value for the grid cell is converted to Mmoles LNO_x using the dimensions of the grid cell. Figure 4 shows the standard error of the mean grid cell LNO_x VCD as a function of the number of OMI pixels used to determine the mean for the Gulf of Mexico region over the months of JJA of 2007 through 2011 assuming a flash threshold of 3000 for the 3 h period prior to the OMI overpass. After applying a seven-point moving average, the standard error remains relatively constant (from ~0.35 Mmoles to ~0.45 Mmoles of LNO_x) as the sample size is increased from 5 to 25. Overall, 10516 (11%) of the 95220 grid boxes (460 days × 23 longitudes × 9 latitudes) have five or more valid OMI retrievals and 679 (total of frequency distribution values for Npixels ≥ 5 shown in Figure 4) also meet the flash threshold. For each of these grid boxes, the standard deviation of the OMI LNO_x values is calculated, converted to Mmoles LNO_x and compared to the mean in that grid box. The average values for the standard deviation and mean are then determined by averaging values from the 679 grid boxes. The resulting values are 1.31 Mmoles for the average standard deviation and 0.60 mol for the average mean, i.e., the coefficient of variation (ratio of standard deviation to mean) of the averages equals 2.2 for this period and region.

In our initial attempt at LNO_x retrieval, we removed the tropospheric background with an independent OMI climatology. This consisted of a 30 day centered average of the standard tropospheric NO_2 from OMI calculated using all high-quality OMI pixels having cloud radiance fraction (CRF) <50%. CRF is an OMI observation of the cloud brightness. Specifically, it is the fraction of OMI-measured radiance coming from the cloudy part of a pixel. A CRF of 0 means the OMI pixel is observing a clear sky, straight through to the ground. A CRF of 1 indicates the OMI pixel is observing exceptionally bright clouds.

We found that this did not properly remove nonlightning NO_2 from the OMI data. In many instances (particularly for pixels with frequent convection), this 30 day climatology was too large, producing negative LNO_x values after subtraction. Such anomalously large background values could result from the AMFs used for the 30 day V_{BG} calculation being too small relative to AMF_{trop} used in equation (1) to compute the LNO_x vertical column. A discrepancy of this nature would occur if the climatological a priori NO_2 profile shapes used in the OMI NO_2 retrieval were in error. These model-derived a priori profiles are only estimates of the true profile shape, especially in regard to boundary layer NO_2 or, to a lesser extent, convective transport to the upper troposphere that is unaccounted for in the model [e.g., *Bucsela et al*., 2008]. Therefore, the calculation of a tropospheric background by this method is particularly difficult.

Given the difficulty in estimating the background, we focus on areas of active or very recently active convection where the lower tropospheric background is minimized. In such regions clouds mask most boundary layer NO_x and some in-cloud NO_x. We note that the remaining NO_x still contains a nonrecent LNO_x component. The possible effects of this component on the results of this study are discussed further in section 4.4. With regard to boundary layer NO_x, we examined LNO_x production over convective storms using thresholds that retained pixels with CRFs greater than 0.7 and 0.9 (or 70% and 90%).

It is not obvious what CRF criterion to use for our regional or global LNO_x analyses. Therefore, to explore the CRF influence on the retrieved column LNO_x, we analyzed 1 day from the Deep Convective Clouds and Chemistry (DC3) campaign. The DC3 experiment was a joint NSF/NASA campaign to understand the role of thunderstorms in upper tropospheric chemistry. An overview of the DC3 field campaign can be found in

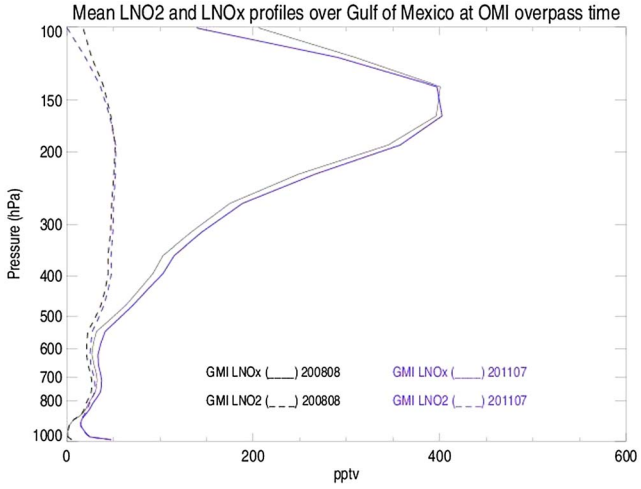

Figure 3. Mean lightning NO_2 and lightning NO_x profiles over the Gulf of Mexico region (100–78°W, 23–31°N) at OMI overpass time over all days of the month determined by taking the difference of vertical profiles between the standard Hindcast FF simulation with the GMI model and a simulation without lightning NO production. The LNO_x (LNO_2) profile is shown with a solid (dashed) line. August 2008 (July 2011) is shown in black (blue).

Barth et al. [2015]. We chose to examine a DC3 flight day because aircraft in situ measurements of NO_x are available, which together with flash locations will aid in determining a CRF threshold to use and how our tropospheric background removal should be treated. The day used in this CRF threshold analysis is 11 June 2012, on which measurements were taken during an active mesoscale convective system over the Central U.S.

In Figure 5a, the OMI CRF values are shown for the region of the 11 June storm. Some pixels (shown in red) have a CRF > 90%. This is indicative of exceptionally bright clouds due to active convection and covers the majority of the storm anvil region as depicted in the GOES IR satellite image in Figure 5b. Unfortunately, the data from the southwestern part of the anvil are missing due to the OMI row anomaly. Figure 5c shows the location of lightning flashes (flash counts uncorrected for DE) from the Earth Networks Total Lighting Network (ENTLN) [*Liu and Heckman*, 2011] for the 3 h prior to the OMI overpass. Figure 5d shows the flight tracks from the DC3 research aircraft color coded by observed NO_2 mixing ratio. The lightning data show that most of the flashes occurred within the CRF > 90% region. However, the aircraft data show enhanced NO_2 well out from the convective core in areas with CRF < 90%. For safety reasons the aircraft did not sufficiently sample the most active parts of the storm, thereby preventing a direct comparison of an aircraft-derived column LNO_2 with that from OMI. From these figures we conclude that inclusion of cloudy grid cells with CRF > 70% is most appropriate for considering the total NO_x from the lightning-producing deep convection, because the CRF > 70% region better matches the enhanced NO_x in the aircraft data than does the CRF > 90% region. However, with the use of CRF > 70%, there is a greater risk that holes in the clouds will allow lower tropospheric (nonlightning) NO_2 to be detected in some pixels. To ensure that our analysis for the Gulf of Mexico (discussed in section 4) is done with pixels over active or recently active convective regions, we perform our calculations using pixels with CRF > 90% and perform a sensitivity calculation using CRF > 70%. In order to minimize the influence of boundary layer pollution, *Choi et al.* [2014] also limited their analysis to

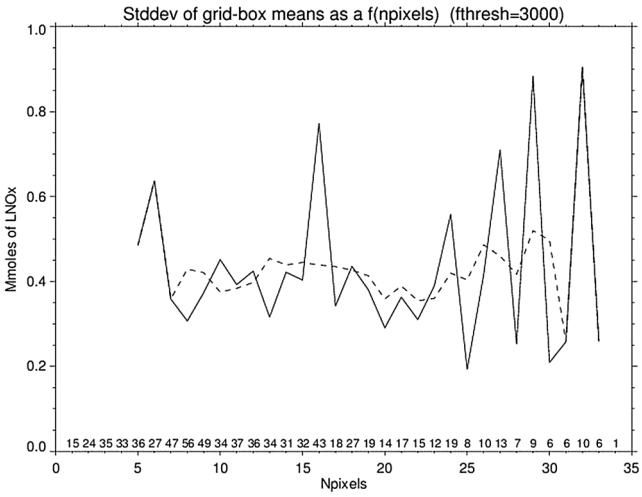

Figure 4. Standard error of V_{LNOx} mean as a function of the number of pixels available to calculate the mean. Distribution determined using all Gulf of Mexico region grid boxes during JJA of 2007 through 2011 with at least 3000 flashes during the 3 h period preceding OMI overpass. The frequency distribution (number of grid boxes) of available pixels is shown in numbers along the bottom of the plot. Seven-point moving average is indicated with the dashed line.

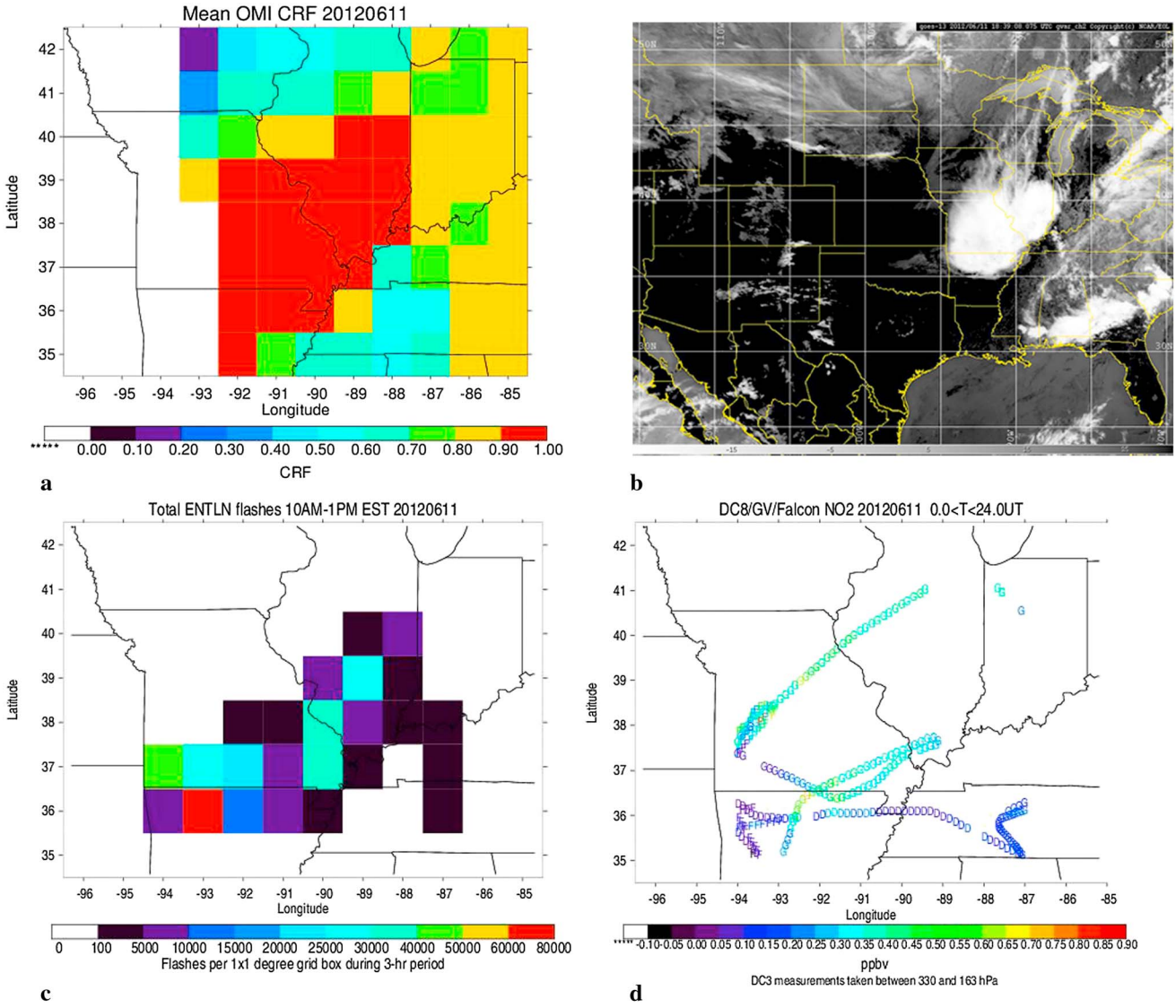

Figure 5. (a) Average OMI CRF on a 1° × 1° grid over a region that includes the 11 June 2012 DC-3 storm. (b) GOES IR brightness temperature image for 1845 UT 11 June 2012. (c) Total ENTLN flashes between 10 A.M. and 1 P.M. EST on 11 June 2012. (d) DC3 research flight tracks (D = NASA DC8; F = DLR Falcon; and G = NCAR G-V) color coded by NO_2 mixing ratio within and in the vicinity of the 11 June 2012 MCS. Note the background NO_2 mixing ratios of ~0.05 ppbv outside of storm in lower left corner of figure.

OMI pixels with a CRF $>$ 90% when deriving free tropospheric NO_2 mixing ratios using a cloud slicing technique. However, we note that even using a CRF $>$ 90% criterion allows a small amount of boundary layer NO_2 to be detected, which affects the magnitude of the background column amount. But using a CRF criterion larger than 90% severely diminishes the number of pixels usable for LNO_x analysis.

Using the thresholds of 70% and 90% eliminates OMI pixels over relatively clear skies and minimal convection, where the majority of the observed column NO_x may be due to lower tropospheric sources. For remaining pixels, we assumed that all retrieved NO_2 originated with lightning and therefore did not remove a tropospheric background. This assumption is most valid over regions where boundary layer sources of NO_x are small such as rural, remote, and/or marine locations. It is supported by cloud-resolved modeling and aircraft data analysis of individual storms over midlatitude rural areas which show 83–90% of NO_x in the anvil to have been produced by lightning occurring in the specific storms studied [e.g., *DeCaria et al.*, 2000, 2005] and 80–95% in storms over the tropics [*Huntrieser et al.*, 2008; *Cummings et al.*, 2013] with the remainder lofted from the lower troposphere. However, part of the background may be NO_x that is transported in the upper troposphere from upwind storms.

We stress that the method described above is valid only for active or recently active storms. We must caution that when attempting to isolate LNO_x in clear-sky regions downwind of storms, subtracting a tropospheric background is absolutely necessary because OMI is observing the total column, from the top of the atmosphere to the surface.

3.5. Method for Estimating LNO_x Production per Flash

The analysis for the Gulf of Mexico region is conducted using 1° latitude × 1° longitude grid resolution. We used all flashes within the 3 h prior to OMI overpass in the Gulf of Mexico spatial domain. The 3 h time period was determined by an analysis of the median 300 hPa MERRA wind speed data by month in relation to grid cell size. Specifically, we estimated the time required to evacuate a grid box by dividing the grid box length by the median 300 hPa wind speed for each month. Wind speeds in the Gulf of Mexico region are on the order of 6–12 m s^{-1}. The grid box length was defined as the square root of the 1° × 1° grid box area. For each month and region, the median wind speed was determined for 15° × 15° regions using 3 h instantaneous 1.25° × 1.25° winds for the time closest to 1330 LT. For the Gulf of Mexico the median residence time in a grid box is approximately 3 h. Therefore, it is assumed that flashes occurring in a 1° × 1° grid box within 3 h prior to OMI overpass contribute to the LNO_x portion of the OMI NO_2 column because most of the LNO_x produced in a grid box will likely still remain and not be transported outside that grid box. LNO_x and 3 h total flashes are summed for all grid boxes within the Gulf of Mexico region where the vertical column of LNO_x is defined (i.e., at least 5 OMI pixels are of high quality and meet the CRF criterion in a grid cell) and a flash threshold is met.

As described in section 3.4, for this analysis, we isolate all pixels with CRFs > 70% and CRFs > 90%. Initial calculations were performed for several thresholds of 1000 flashes or less per 3 h. However, we ultimately decided to use a threshold of 3000 flashes per 3 h to ensure that the NO_2 from LNO_x exceeded the background NO_2. The background was estimated using upper tropospheric NO measurements from the CRYSTAL-FACE (Cirrus Regional Study of Tropical Anvils and Cirrus Layers—Florida Area Cirrus Experiment) mission in south Florida in July 2002 [*Ridley et al*., 2004] and NO_2 measurements from a NCAR G-V flight (25 June 2012) over the Gulf of Mexico during DC3. The background values from these flights were 100–300 pptv NO and 100 pptv NO_2, respectively. The NO value was converted to NO_2 using the assumption that NO_2 comprised 23% of NO_x, which was the summertime mean for the 200–500 hPa layer in the Gulf of Mexico region from the Hindcast FF simulation with the GMI model. The moles of NO_2 associated with these background values were then calculated for the 200–500 hPa layer for a 1 × 1 grid box. The moles of NO_2 associated with LNO_x were then calculated using values of LNO_x production per flash of 100 to 200 mol. The background and LNO_x moles of NO_2 were compared and found to be comparable for flash rates of 1500–4000 flashes per 3 h. In order to maximize the signal while maintaining an adequate number of events, we chose a flash threshold of 3000 flashes for this analysis. This threshold is smaller than that used in the *Beirle et al*. [2010] analysis (1 flash per km^2/h), which is roughly equivalent to 10,000 flashes in our grid cells. Therefore, we should be able to retrieve LNO_x for a greater number of cases. We use two methods of estimating the monthly mean LNO_x production per flash: (1) summing the OMI LNO_x production over the region and over the month analyzed and dividing by the sum of flashes occurring in these grid boxes over the month and (2) computing the slope and intercept from linear regression of daily totals of OMI LNO_x and flashes over the region. The summation method can be also applied on a daily basis.

The JJA 2008 WWLLN detection efficiency is relatively low as discussed in section 3.2. For this reason, we chose to expand our initial analysis to include JJA 2011, a season when WWLLN detection efficiency is better for the Gulf of Mexico. However, OMI retrievals in JJA 2011 are more affected by the row anomaly than OMI retrievals in JJA 2008. Specifically, for a flash threshold of 3000, the number of 1° × 1° grid boxes with at least 5 pixels equaled 209 in JJA 2008 and 57 in JJA 2011. Therefore, the standard error was larger in JJA 2011 than in JJA 2008.

4. Results

4.1. Estimate of LNO_x Production in Summer 2008

Our LNO_x algorithm was applied for all days during JJA 2008 over the Gulf of Mexico region. In Figure 6, the daily means of LNO_x production (moles per flash) using the summation method are plotted for the region for each day of the season for CRF > 70% and CRF > 90% using a threshold of 3000 flashes per grid cell. The daily mean LNO_x production (moles per flash) values are mostly in the range from ~50 to 250 mol per flash. The

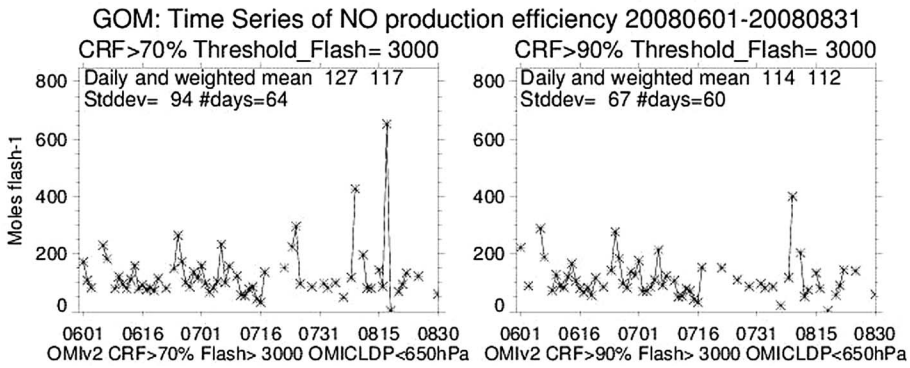

Figure 6. Time series plot of OMI LNO_x production per day over the Gulf of Mexico for JJA 2008 with (left) CRF > 70% and a flash threshold of 3000 flashes per 3 h using the summation method. (right) Same as Figure 6 (left) except for CRF > 90%.

number of days in this season with data meeting all criteria is 64 for CRF > 70% and drops to 60 for CRF > 90%. The mean (each day weighted by the number of grid cells of data available) and standard deviation of the daily values (Table 2) are 117 ± 94 mol per flash for CRF > 70% and 112 ± 67 mol per flash for CRF > 90%. The seasonal LNO_x moles per flash values for the region for JJA 2008 are near the lower end of the range of literature values (Table 1). In Figures 7 and 8, the JJA 2008 seasonal mean production of LNO_x, mean WWLLN flashes, and mean LNO_x moles per flash for each grid cell for the 3000 flash threshold are shown for CRF > 70% and CRF > 90%, respectively. Flashes tend to maximize on the land areas surrounding the Gulf or just offshore. However, LNO_x production per flash does not appear to have any particular geographic pattern. We note that the spatial agreement between WWLLN flashes and LNO_x is only moderate and that some low values of production per flash are associated with high flash rates and vice versa. The moderate agreement is likely due to noise in the OMI LNO_x VCD and WWLLN flashes, but it is to some extent consistent with recent studies that suggest that high flash rate storms have shorter flash lengths and possibly smaller values of production per flash than low flash rate storms [e.g., *Bruning and MacGorman*, 2013; *Mecikalski et al.*, 2015].

Figure 9 shows the percentage of 1° × 1° grid cells with valid LNO_x data that enter the analysis for thresholds of 100, 300, 500, 1000, and 3000 flashes per 3 h prior to OMI overpass. Roughly 10–15% of grid cells with valid LNO_x data have >3000 flashes per 3 h.

The seasonal mean values shown in Table 2 increase by <5% when the CRF criteria are relaxed from 90% to 70%. It is likely that with the CRF > 70% condition some pixels are viewing into the lower troposphere, thereby detecting nonlightning NO_x (especially over land areas) and high biasing the LNO_x production. However, excluding pixels with CRF values between 70 and 90% could lead to a low bias as the LNO_x anvil is likely larger than the region of active lightning and may extend into the region of the cloud with low to moderate flash rates and CRF values between 70 and 90% (see Figure 5).

Figure 10 presents a scatterplot and linear regression analysis for the daily moles of OMI LNO_x and WWLLN flash data over the region during JJA 2008 for CRF > 90% and a flash threshold of 3000 flashes per 3 h. The slope of the regression is 115 ± 25 mol per flash with a correlation of 0.77. The production per flash value provided by the slope is very close to that (112 ± 67 mol per flash) obtained by the summation method for CRF > 90%. The *y* intercept is very close to zero, which may indicate little to no interference from background sources.

Table 2. Seasonal Mean LNO_x Production (Moles per Flash) From the Summation Method Using the 3000 Flash Threshold and Two CRF Criteria Over the Gulf of Mexico During JJA 2008[a]

CRF Criterion	Mn	wMn	σ	N
70%	127	117	94	64
90%	114	112	67	60

[a]The "Mn", "wMn", "σ", and "N" columns show the mean of the daily averages, the mean of all grid boxes with data, the standard deviation of the daily averages, and the number of days for which data are available.

4.2. Estimate of LNO_x Production in Summer 2011

The same analysis as outlined in section 4.1 was completed for JJA 2011. Results from the analysis using pixels with a CRF > 90% are discussed for JJA 2011, although a similar analysis using pixels with a CRF > 70% was also conducted (figures not shown). Due to the OMI row anomaly, analysis

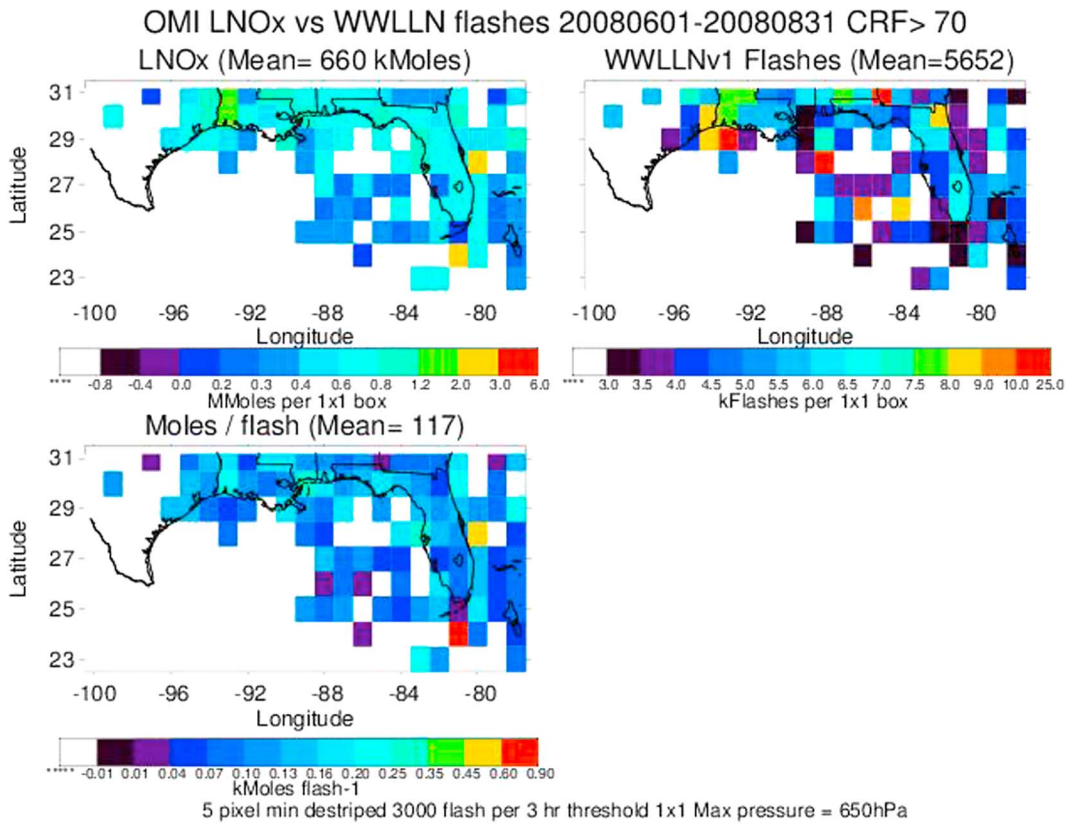

Figure 7. Maps of 1° × 1° gridded values of (top left) mean OMI LNO_x for JJA 2008, (top right) gridded mean WWLLN 11:00–13:59 LT flashes for JJA 2008, and (bottom left) gridded monthly mean LNO_x production per flash based on summation for CRF > 70% and a 3000 flash threshold.

during JJA 2011 requires many days to be removed from each month of this seasonal average. Valid LNO_x was available for only 30 days during this season. The time series plot (Figure 11) shows daily LNO_x production per flash using the summation method for each day of JJA 2011 with the 3000 flash threshold. Note also that there are a few days when LNO_x values are between zero and 50 mol per flash. This result is not surprising given the *Beirle et al.* [2010] analysis which found many cases of significant numbers of flashes but no LNO_x signal in the SCIAMACHY data, for reasons unknown. For example, if indeed IC flashes produce much less NO_x per flash than CG flashes and storms on a given day were dominated by IC flashes, a relatively small mean value would result. The gaps in the data are indicative of days where the flash threshold was not met or the OMI row anomaly affected too much of the Gulf of Mexico region for analysis to proceed. The row anomaly requires many pixels to be categorized as missing data. As a result of the decreased OMI coverage, a lesser number of storms are sampled. Assuming a CRF threshold of 90% for the summation method, the weighted monthly mean over the 30 available days of JJA 2011 was 102 ± 144 mol per flash. The mean value is very close to that for JJA 2008 (112 mol per flash) despite differences in detection efficiency and OMI coverage between the time periods. For these two seasons, these two factors had little influence on the seasonal mean LNO_x production value for the Gulf of Mexico region.

Figure 12 shows maps of seasonal mean production of LNO_x, mean WWLLN flashes, and mean production of LNO_x per flash for each grid cell for JJA 2011 using a CRF threshold of 90%, a 3 h flash accumulation period prior to the OMI overpass, and a flash threshold of 3000 flashes. Note the much lesser number of grid cells for which data are available in JJA 2011 compared with JJA 2008. It can also be noted that grid cells with particularly large values of flashes often tend to be found both along the coast and just offshore.

Figure 13 presents a scatterplot and linear regression of the daily values of LNO_x and WWLLN flashes in the region during JJA 2011 for the 3000 flashes per 3 h threshold. The slope of the regression is 69 ± 35 mol per flash with a correlation of 0.61 (somewhat lower than for JJA 2008). This estimate is smaller than the

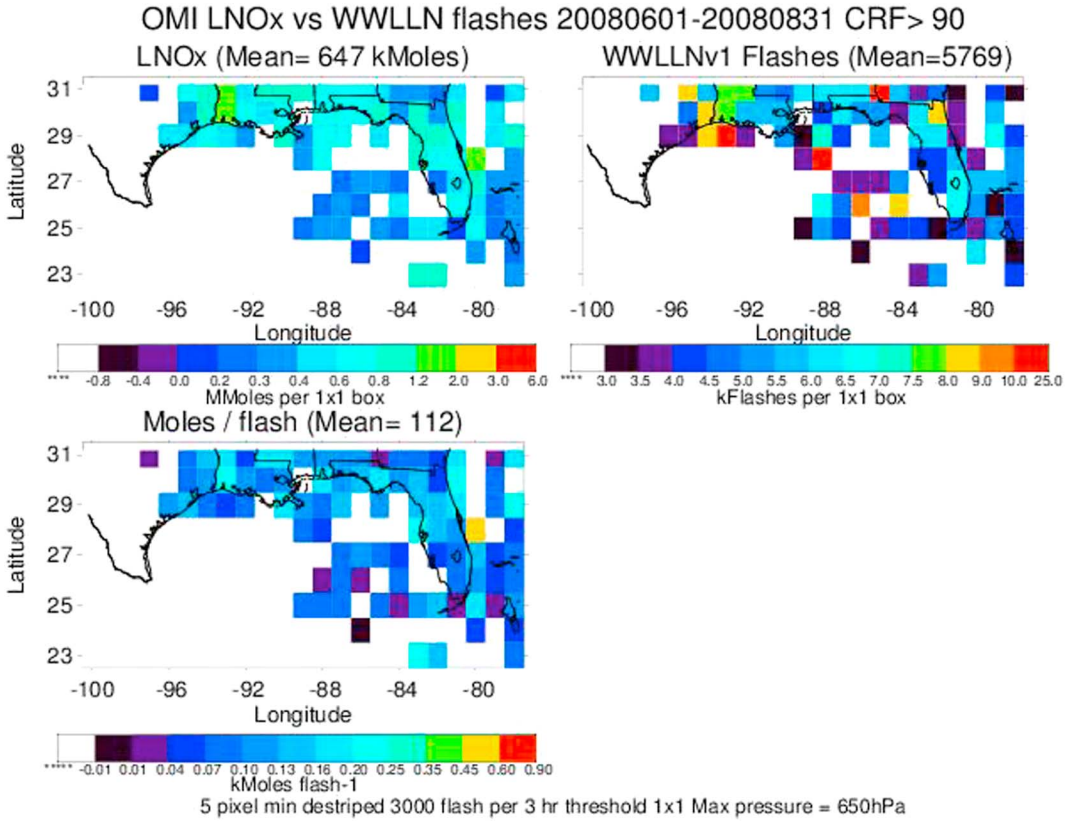

Figure 8. Same as Figure 7 except for CRF > 90%.

corresponding estimate using the summation method. The predominance of on-shore or near-shore grid cells involved for this season may lead to the significant difference between the summation and regression results. For this season the regression approach attributes a portion of the LNO_x (i.e., the *y* intercept) to sources other than lightning occurring in the 3 h prior to OMI overpass (most likely upwind lightning).

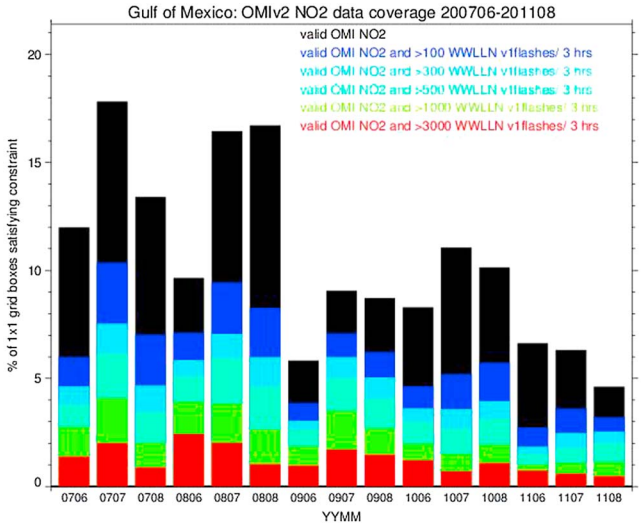

Figure 9. Percentage of grid boxes over Gulf of Mexico region having valid OMI LNO_x (>5 pixels with CRF > 90% in a grid box; black) and satisfying the thresholds 100 (blue), 300 (light blue), 500 (turquoise), 1000 (green), and 3000 (red) flashes per 3 h prior to OMI overpass.

4.3. Estimates of LNO_x Production in All 2007–2011 Summer Months

Analyses of the summer months of other years within the Gulf of Mexico region are necessary to determine if the LNO_x production per flash values are consistent over a longer period. We have conducted analyses for JJA of 2007 through 2011 similar to those presented above in detail for JJA 2008 and JJA 2011 based on the summation and regression methods. Figure 14 shows the JJA seasonal results for the summation method and regression method by year over all five years for the CRF > 90% and 3000 flash threshold. The overall mean over these five summer seasons is 103 mol per flash for the

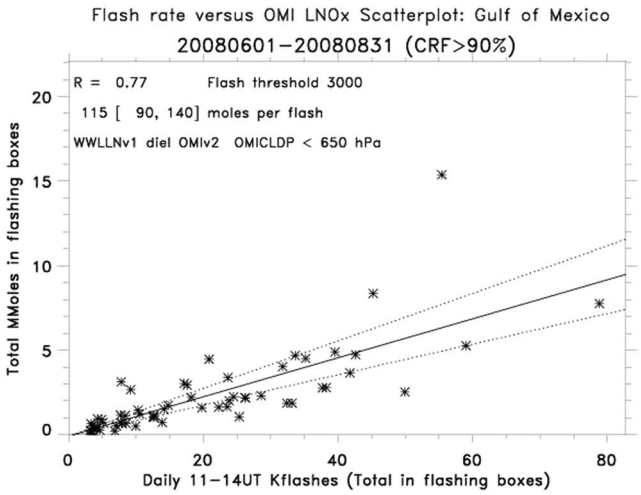

Figure 10. Scatterplot and linear regression of daily values of total MMoles LNO_x summed over grid cells with flashes versus Kflashes in the 3 h prior to OMI overpass for JJA 2008 with CRF > 90% and flash threshold of 3000 flashes.

summation method, and the mean for the regression method is 91 mol per flash. Interannual variability of LNO_x production per flash is small with the standard deviation over the five years equaling 10 mol per flash for the summation method and moderate for the regression method (24 mol per flash). Therefore, we conclude that our OMI analysis yields mean LNO_x production over the Gulf of Mexico over five summers in the ~91 to 103 mol per flash range, but individual summers can have means ranging from 91 to 112 mol per flash for the summation method and from 69 to 120 for the regression method.

4.4. Estimation of Uncertainties

There are several types of uncertainties associated with our estimates of LNO_x production per flash. The uncertainties (summarized in Table 3) stem from the OMI data itself, from elements of our LNO_x algorithm, and from our treatment of the WWLLN data. We provide our best estimates of the errors associated with each component of our calculation in Table 3 and as described below. A more detailed treatment of the uncertainties in estimating LNO_x from OMI is given by *Bucsela et al*. [2010].

Errors are present in the spectral fit used to obtain OMI slant columns of NO_2. The random uncertainties in the OMI slant column retrievals for individual pixels become negligible compared with systematic uncertainties when the data are averaged over a month, as we are doing in this analysis. Systematic errors in the slant columns due to the spectral fit performed at KNMI [*Boersma et al*., 2011] have been shown to be significant

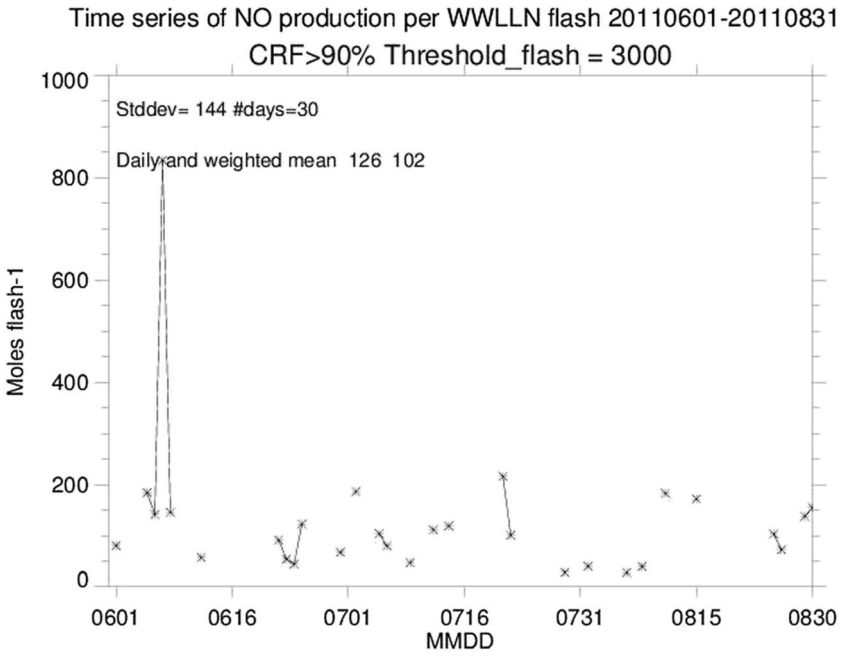

Figure 11. Time series plot of OMI LNO_x production per day over the Gulf of Mexico for JJA 2011 with CRF > 90% and a flash threshold of 3000 flashes per 3 h using the summation method.

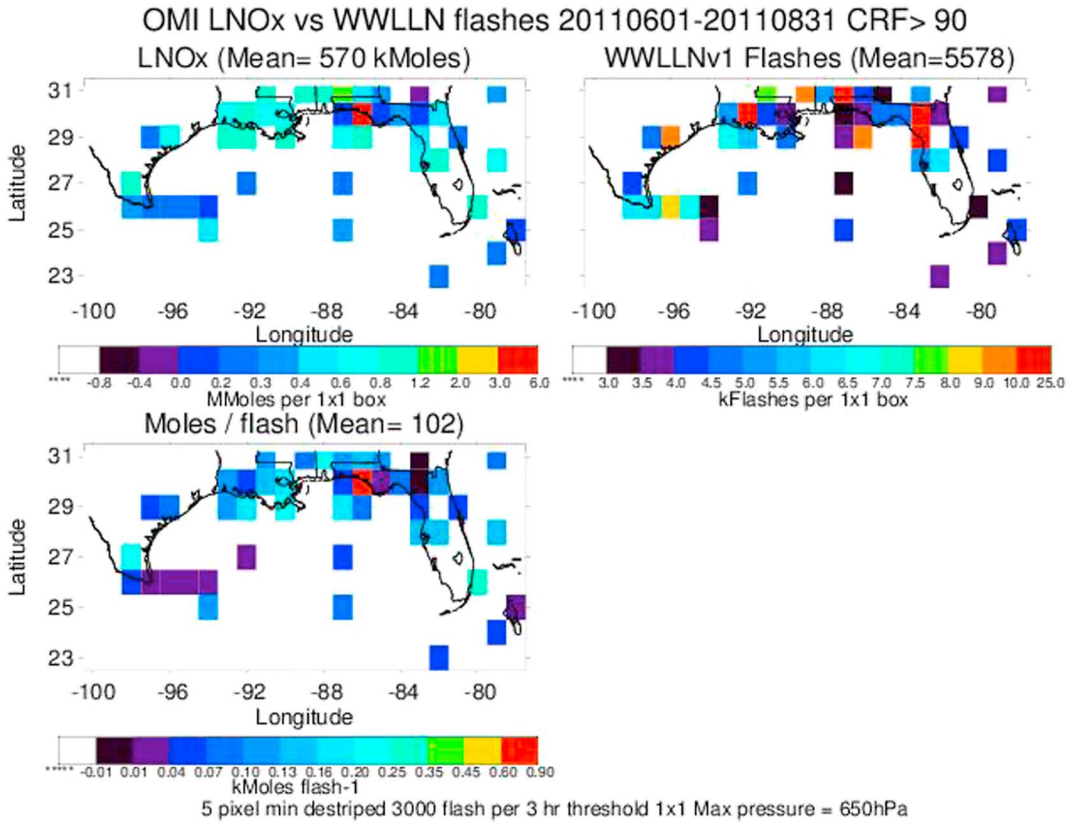

Figure 12. For JJA 2011, maps of 1° × 1° (top left) gridded mean OMI LNO_x, (top right) gridded mean WWLLN 11:00–13:59 LT flashes, and (bottom left) gridded mean LNO_x production per flash based on the summation method for CRF > 90% and a 3000 flash threshold.

especially over rural/remote areas [*Marchenko et al.*, 2015]. At the magnitudes of tropospheric NO_2 columns resulting from lightning in this study ($1–4 \times 10^{15}$ molecules cm^{-2}) the spectral fitting error results in a ~20–30% high bias in the tropospheric vertical columns in summer. However, comparison of tropospheric column estimates over highly reflective clouds from the version 2.1 OMI standard product used in this study with a preliminary version 3 product that uses an improved method of performing the spectral fit does not indicate the bias shown by *Marchenko et al.* [2015]; i.e., no systematic bias is seen in the slant columns; therefore, no bias correction for spectral fitting errors is made in this study, but an uncertainty of ±15% is assumed.

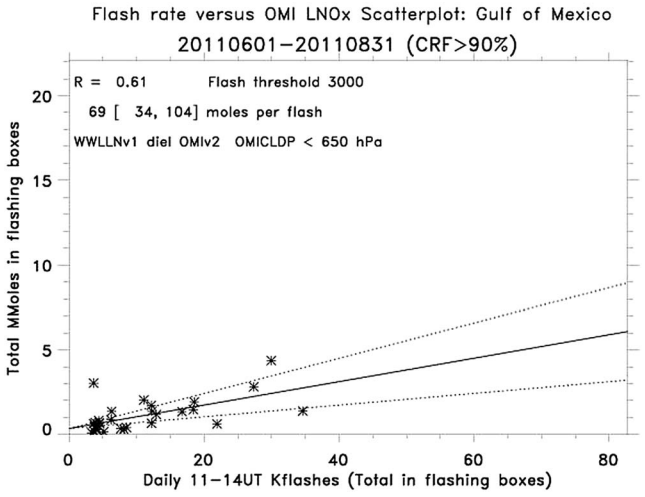

Figure 13. Scatterplot and linear regression of daily values of total MMoles LNO_x summed over grid cells with flashes versus Kflashes in the 3 h prior to OMI overpass for JJA 2011 with CRF > 90% and flash threshold of 3000 flashes.

There are four primary aspects of our LNO_x estimation algorithm that may introduce uncertainties. They are the detection of LNO_x in the lower portion of the cloud, the stratospheric NO_2 term, the tropospheric background term, and our use of only the CRF > 90% pixels. The OMI retrieval

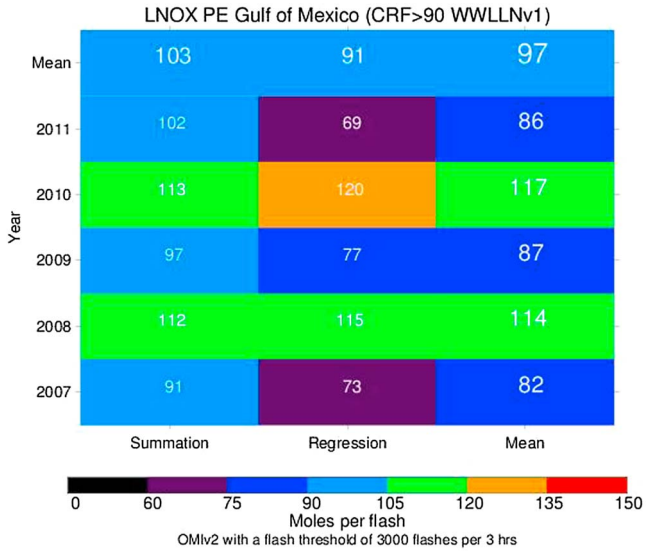

Figure 14. Summation-based and regression-based OMI LNO_x production per flash over the Gulf of Mexico for JJA 2007–2011 using a CRF > 90% criterion and a 3000 flash threshold. Means for the individual methods and years are shown in a larger font on top and right, respectively. Overall mean is shown in the largest font on top right.

of NO_2 over clouds is restricted to the region above the cloud top pressure (optical centroid pressure, OCP) estimated from OMI using rotational Raman scattering [*Vasilkov et al.*, 2008]. The OCP is often substantially larger than the IR-derived cloud top pressure, but significant amounts of LNO_x may exist below the OMI cloud top. While only the NO_2 above the OCP is actually "seen" by OMI, we implicitly account for the entire LNO_x column in the air mass factor AMF_{LNOx}. The LNO_x profile shape used in the AMF defines a below-cloud fraction of the LNO_x column, which is then scaled by the measured amount above the cloud. The sum yields an estimate of the total LNO_x column. Figure 15 presents a frequency distribution of the OMI optical centroid pressures observed over the Gulf of Mexico region during June, July, and August of 2007 to 2011. These pressures ranged from ~200 hPa to 650 hPa, with the most frequent values in the 450–500 hPa bin. *Ott et al.* [2010] conducted cloud-resolved chemistry thunderstorm simulations and generated typical profiles of the fraction of total mass of LNO_x present in a storm as a function of altitude and climatic regime. Using the profile for the subtropics (generated from simulations of Florida storms), it appears that ~12% and ~82% of LNO_x would be located below OMI optical centroid pressures of 625 hPa and 225 hPa, respectively. For the most frequent cloud pressure (475 hPa bin), ~30% would be below this level. In our study, the profiles used to generate the AMF_{LNOx} are based on a GMI climatology obtained by averaging profiles on days with the highest amounts of LNO_x. These profiles were chosen on the assumption that they better represent profiles in active thunderstorms than those of straight monthly means. Like the Ott et al. profile, the GMI simulations indicate that approximately 25–30% of the LNO_x column lies below the OCP. Differences between the GMI and Ott et al. profiles lead to an uncertainty on the order of 5–10% in the resultant AMF_{LNOx}. This potential source of error propagates into an uncertainty in our retrieved LNO_x amount, and we conservatively estimate this to be ±10%

Bucsela et al. [2013] describe the method used to derive the stratosphere in version 2 of the standard OMI NO_2 algorithm. *Bucsela et al.* [2010] compared methods of estimating the stratospheric component of the vertical NO_2 column and found differences on the order of 1×10^{14} molecules cm^{-2}, a value appropriate for the tropics. *Bucsela et al.* [2013] estimated the stratospheric column uncertainty at 2×10^{14} molecule cm^{-2} in

Table 3. Sources of Uncertainty in the LNO_x Production per Flash Estimates

Type of Uncertainty	Mean Bias (%)	Uncertainty (%)
Random errors in slant columns	~0	0
Systematic errors in slant columns	~0[a]	±15[a]
LNO_x below OMI optical centroid pressure	~0	±10
Stratospheric vertical column amount	~0	±35 to 40
Tropospheric background	18	±15
WWLLN detection efficiency	~0	±30
Flash counting window	~0	±15
Net	18	±55

[a]The mean bias and uncertainty are preliminary estimates (see beginning of section 4.4), and these terms will be further studied when the OMI NO2 version 3 product, which includes a new retrieval of the slant columns, is finalized.

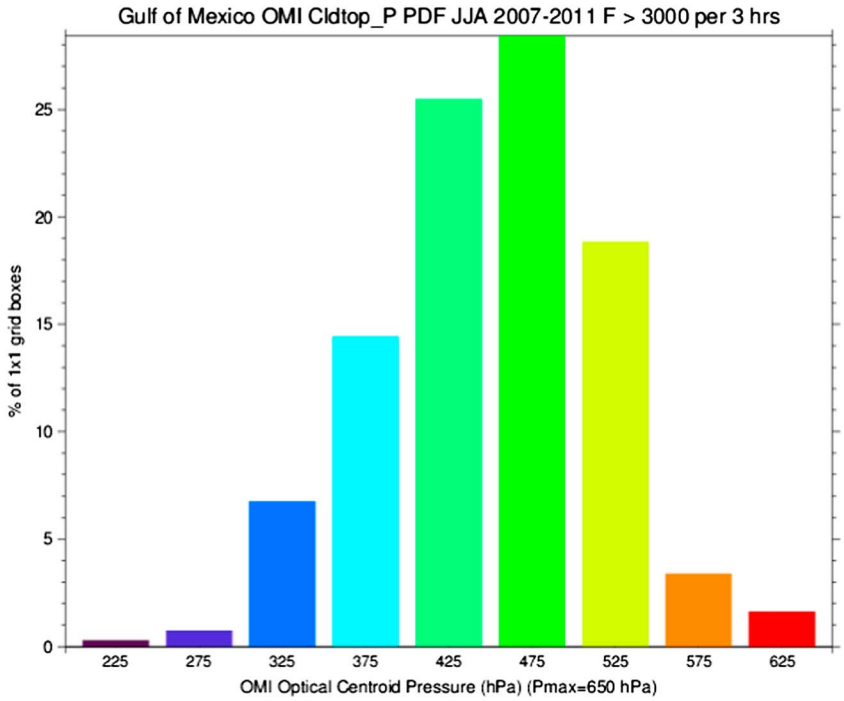

Figure 15. Frequency distribution of OMI Optical Centroid Pressures for the June, July, and August period of 2007 through 2011 for grid cells with >3000 flashes/3 h prior to OMI overpass.

polluted areas, which tend to be associated with midlatitudes. We have performed a sensitivity study of the impact of these estimates of stratospheric uncertainty on the LNO_x production per flash. We performed LNO_x retrievals for two months (July 2008 and August 2011) assuming the OMI standard stratospheric NO_2 product as the base case and sensitivity retrievals using stratospheric NO_2 columns that are plus and minus each of the two aforementioned values. The resulting LNO_x production per flash values from the sensitivity simulations were compared with the base case estimate. We found that the stratospheric uncertainties yielded LNO_x differences of ~25% and ~50%, respectively, for the two values of uncertainty that were tested. The 1×10^{14} value is appropriate for the tropics where stratospheric gradients are relatively weak, and the 2×10^{14} value is more appropriate for midlatitudes where the stratospheric NO_2 is greater and stronger gradients exist. Therefore, for the subtropical Gulf of Mexico region the most likely uncertainty in the LNO_x due to the stratospheric uncertainty is ~35–40%.

In our calculations of LNO_x in sections 4.1 through 4.3 we have assumed a zero tropospheric background due to uncertainty in how it should be determined. We have explored several ways of estimating this background. The high CRF criterion effectively removes boundary layer pollution influence, as evidenced by the plots in Figure 16. The OMI LNO_x does not demonstrate correlation with the OMI standard product tropospheric NO_2, which is dominated by boundary layer pollution, or with the EDGAR (Emission Database for Global Atmospheric Research, release version 4.2. http://edgar.jrc.ec.europa.eu) NO_x emissions. This region includes several major urban areas, including Houston, New Orleans, Tampa/St. Petersburg, and Miami. Therefore, it appears that these urban areas had no substantial pollution influence on our LNO_x retrievals. However, upper tropospheric NO_x from upwind lightning earlier in the day or from previous days will still be present. Background may be accounted for implicitly in the regression method (through the *y* intercept) but is included with the fresh LNO_x in the summation method. The *y* intercept was near zero for JJA 2008 but was significantly positive for JJA 2011. A significant background in this region is plausible given the 2 to 5 day upper tropospheric lifetime of NO_x [*Olson et al.*, 2005; *Bertram et al.*, 2007; *Cooper et al.*, 2006] and the climatology of this region that favors recirculation around a subtropical anticyclone [e.g., *Cooper et al.*, 2006, 2007].

As noted in section 3.4, cloud-resolved modeling of individual storms in nonurban areas constrained by anvil aircraft observations has indicated that thunderstorm anvil NO_x may be composed of about 5–20% from sources other than lightning in the simulated storm. The mean of the range (a value of ~12%) may be

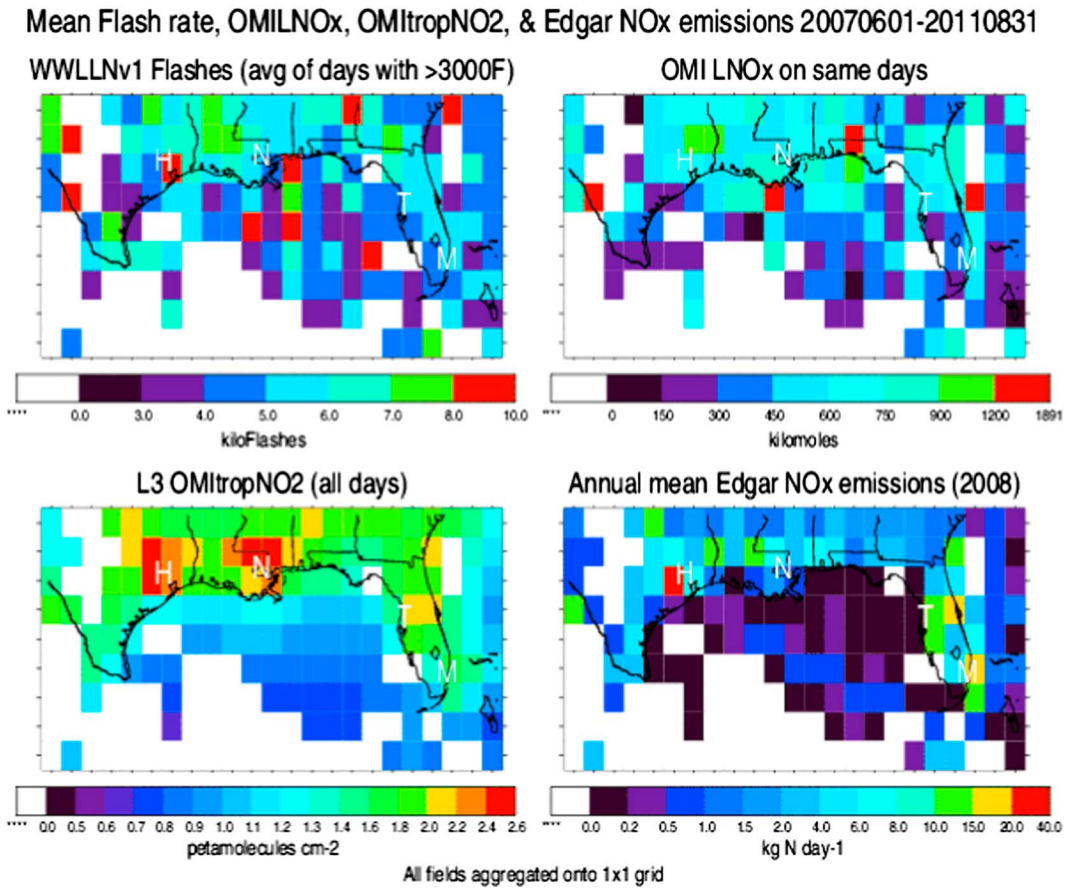

Figure 16. Comparison of spatial distributions of detection efficiency-adjusted (top left) WWLLN flashes, (top right) OMI LNO_x, (bottom left) level 3 OMI standard product tropospheric NO_2, and (bottom right) EDGAR NO_x emissions over the Gulf of Mexico region. The time periods shown are June through August 2007–2011 for WWLLN flashes, OMI LNO_x, and OMI tropospheric NO_2 and 2008 for EDGAR emissions. Grid boxes shown in white are locations where the flash threshold was not met on days with valid OMI data. H = Houston, TX; N = New Orleans, LA; T = Tampa, FL; and M = Miami, FL.

appropriate for the Gulf of Mexico (less than over the continental U.S. but greater than the remote tropics). Therefore, previous cloud-resolved modeling suggests that our estimates of LNO_x production per flash may be biased high by this amount. However, perhaps the best estimates for upper tropospheric background may come from the few snapshots of NO and NO_2 data measured by research aircraft in the Gulf of Mexico region. In section 3.5 we used these data from CRYSTAL-FACE and DC3 in deriving the 3000 flash threshold for use in our analysis. The CRYSTAL-FACE data showed that outside the storms in this region NO typically was 100–300 pptv between 10 km and the tropopause, while within the storm anvils NO was greater than 3000 pptv over broad horizontal regions. These results suggest that typically, a very small background as a percentage (~3–10%) of the lightning signal is present in this region. However, there were some cases where upwind storms on the same day contributed 1000 pptv or more NO in the vicinities of sampled anvils, implying a >30% background. One flight of the NCAR G-V aircraft was conducted over the Gulf of Mexico during the DC3 field program. This flight encountered a major NO_x plume, which was likely due to fresh LNO_x from active convection over the central portion of the Gulf. The remainder of the flight over the Gulf can be considered as background but may be a somewhat high biased background due to the presence of biomass burning tracers. Over the 9 to 12.5 km altitude range, the background averaged ~33% of the mean value in the LNO_x outflow.

Therefore, it is quite likely that a background component does exist in our LNO_x estimates, which induces a high bias, particularly in the summation method. However, significant uncertainty (range of 3% to >30%) exists in how to best characterize background NO_x in this region.

Use of the CRF > 90% criterion may induce a bias due to lack of consideration of LNO_x existing in portions of the anvil where CRF is less than 90% (see section 3.4). Typically, the size of a thunderstorm LNO_x anvil is larger than the size of the region containing flashes. However, we use the mean of the OMI pixels within a grid cell that contains the flashes, not the sum of the pixels, which avoids the need to add the LNO_x outside the CRF > 90% region. Therefore, we assume negligible bias from this aspect of our retrieval scheme.

Uncertainty also exists in the flash rates that we have derived from WWLLN data. These uncertainties stem from the estimation of WWLLN detection efficiency and from the length of time over which flashes are counted prior to OMI overpass. The detection efficiency-adjusted flash rates used here are 25–30% lower than ones derived from an alternate scheme, which uses a different method of diel adjustment, different weighting periods for each month, and the relative detection efficiencies of *Hutchins et al.* [2012]. However, it is uncertain which method is most realistic.

We have used a 3 h window (the 3 h prior to OMI overpass) for counting WWLLN flashes for use in our LNO_x analysis. This length of time was based on the monthly median 300 hPa wind speed from the MERRA reanalysis as described in section 3.5. However, there is month-to-month variability in these wind speeds and of course daily variability as well. We have performed sensitivity calculations using windows of 2 h and 4 h in length and found that the 2 h window yields LNO_x per flash from 18% to 27% larger than for a 3 h window for the summation and regression approaches. The 4 h window yields LNO_x production estimates 12%–13% smaller than those for the 3 h window. We assume an uncertainty of ±15%.

Our LNO_x per flash estimates contain a bias related to neglect of any tropospheric background. However, the bias in relation to the preliminary version 3 OMI slant column values was found to be negligible in the case of small tropospheric values over cloudy scenes. To correct for the background bias, we subtract the midpoint (18%) of the background range discussed above. We apply this bias correction to the average of the five summer means from the summation and regression methods, namely, 97 mol LNO_x per flash. The bias adjustment yields a corrected value of 80 mol per flash. We can estimate an overall uncertainty in this value as the square root of the sum of the squares of the individual uncertainties in Table 3 and arrive at a net uncertainty of ±55%. Application of this uncertainty to the 80 mol per flash results in a final range of 80 ± 45 mol per flash.

5. Discussion

The seasonal mean values of LNO_x production per flash derived in section 4.4 fall near the lower end of current literature estimates (Table 1). These values are smaller than those derived from cloud-resolved chemistry modeling but more closely correspond to estimates from aircraft data and some other satellite data.

The Gulf of Mexico region lies on the border between the tropics and midlatitudes, but we find that our LNO_x production per flash estimates more closely correspond with the literature values found for the tropics (generally <250 mol per flash), as detailed in Table 1. *Beirle et al.* [2006] studied LNO_x production from a storm system in the Gulf of Mexico using GOME and NLDN data. Their findings ranged from 32 to 240 mol per flash. The summation and regression values from our analysis are the lower half of this range. The very coarse spatial resolution of the GOME data could lead to the small values obtained by *Beirle et al.* [2006]. The global analysis using SCIAMACHY NO_2 data by *Beirle et al.* [2010] found storms with LNO_x production of ~200 mol per flash over the western Atlantic near the coast of North America and in the Gulf of Mexico. Our seasonal mean estimates are less than the *Beirle et al.* [2010] values, but some individual grid cells (Figures 8 and 12) have seasonal LNO_x production per flash in the ~200 mol per flash range. Thus, our findings are in general agreement with the *Beirle et al.* [2010] analysis in this region. Table 1 also lists values of LNO_x production that were derived from in situ observations in the Gulf of Mexico region. Estimates from in situ aircraft NO data by *Ridley et al.* [2004] in CRYSTAL-FACE were 55–110 mol per flash for moderate flash rate storms and 282–382 mol per flash for high flash rate storms. Estimates from the two CRYSTAL-FACE storms simulated by *Ott et al.* [2010] and constrained by the Ridley et al. data were 590 and 700 mol per flash. Our OMI-based estimates are in the range of the set of Ridley et al. values estimated from aircraft measurements from moderate flash rate storms. Although *Koshak* [2014] found large differences in LNO_x production on a per flash basis between IC and CG flashes, the weighted mean over 9 years of northern Alabama data is 227 mol per flash. Our seasonal means over the summers of 2007 to 2011 are smaller than this value.

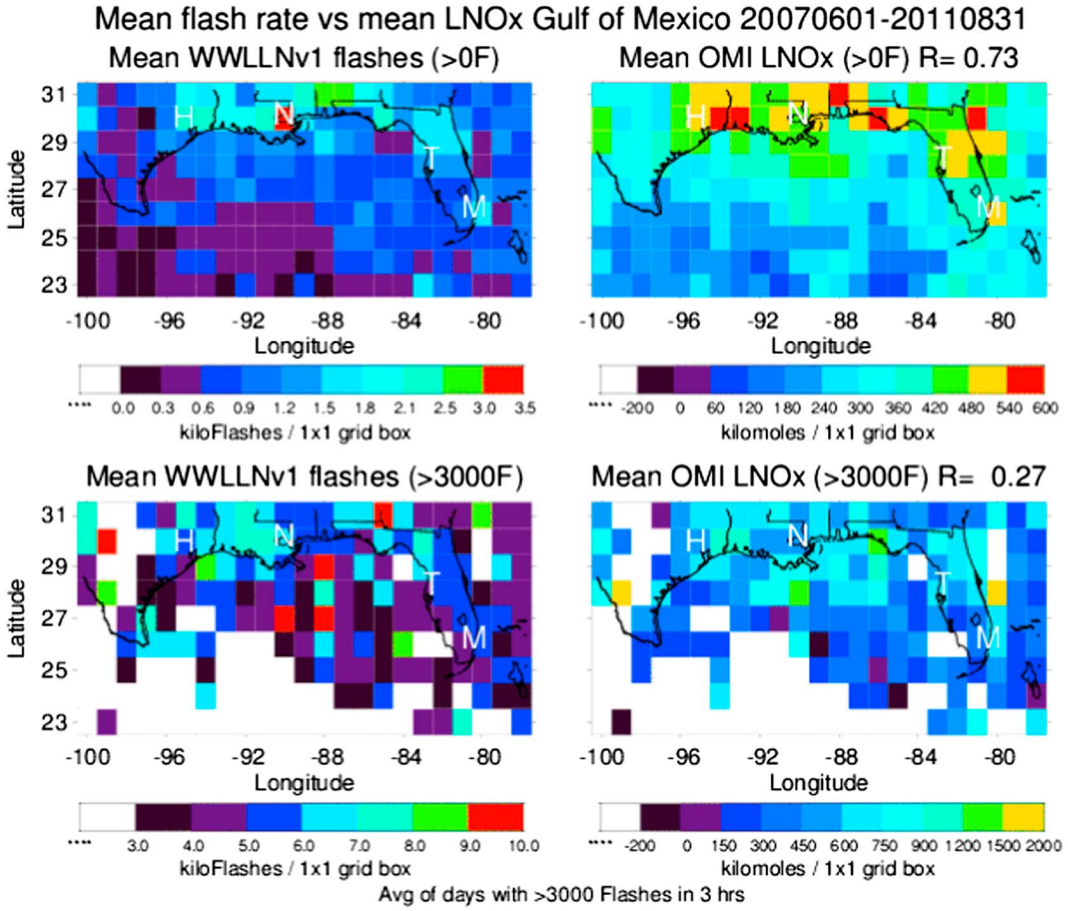

Figure 17. Spatial patterns of detection efficiency-adjusted (left column) WWLLN flashes and (right column) OMI LNO_x are compared for grid boxes with (top row) at least one flash and (bottom row) at least 3000 flashes over the Gulf of Mexico region during JJA 2007 through 2011. Correlations between the patterns are shown in the upper right corners of the OMI LNO_x plots.

The relatively high temporal correlations between daily total flashes and daily total OMI LNO_x shown in Figures 10 and 13 scatterplots do not imply that WWLLN flash rates are highly spatially correlated with OMI LNO_x. Indeed, the temporal correlations are somewhat misleading because the number of grid boxes contributing to the daily totals varies from day to day and enhances the correlations. Figure 17 compares the JJA 2007–2011 spatial agreement between WWLLN flashes and OMI LNO_x for a CRF threshold of 90% and flash thresholds of 1 (Figure 17, top row) and 3000 (Figure 17, bottom row) per 3 h. Overall, there is a modest correlation between WWLLN flashes and OMI LNO_x. As expected, the spatial agreement is much better for the low flash threshold (0.73) than the high flash threshold (0.27) because the low threshold samples a larger range of flash values and associated LNO_x values. Peak flash rates and OMI LNO_x production both can be seen along the coastal areas of Texas, Louisiana, Mississippi, Alabama, and Florida. The modest spatial correlation is mostly due to noise in the OMI LNO_x VCDs and WWLLN flash rates. However, an extremely high correlation is not expected, especially if production per flash decreases at larger flash rates as suggested by the flash extent results of *Bruning and MacGorman* [2013] and *Mecikalski et al.* [2015].

6. Conclusions

An algorithm for retrieval of LNO_x from OMI has been developed for application over active or recently active convection. It uses OMI pixels with CRF $>$ 90% to ensure that boundary layer pollution is blocked from view. We have applied this algorithm on a daily basis for $1° \times 1°$ grid cells over the Gulf of Mexico for 15 summer months from 2007 to 2011 and obtained seasonal mean estimates of LNO_x production per flash for the region

using detection efficiency-adjusted WWLLN data. In order to ensure that we are detecting LNO_x signals above background and to minimize noise, LNO_x production efficiency calculations are limited to grid boxes where the flash rate exceeds 3000 flashes during the 3 h period prior to OMI overpass, where 3 h is an estimate of the residence time of LNO_x in a grid cell in this region. Two methods of computing the seasonal mean LNO_x production per flash were used: summation over the grid cells meeting the above criteria and over the days of the season and regression of the daily totals of flashes and LNO_x over the region.

The individual seasonal mean values of LNO_x production from the two methods (69 to 120 mol per flash) ranged from ~60 to ~100 mol per flash after adjustment for the known bias due to tropospheric background. The mean LNO_x production per flash over the five summer seasons and the two methods is 97 mol per flash, which becomes 80 mol per flash after correcting for the bias. Considering the uncertainties due to systematic slant column errors, LNO_x below the OCP, stratospheric column amount, the tropospheric background, the WWLLN detection efficiency, and the flash counting window, which together amount to ±55%, we arrive at a final range of 80 ± 45 mol per flash. We believe that the five summer season mean of ~80 ± 45 mol per flash that includes consideration of the biases and uncertainties is the most likely range for this region based on the OMI data. WWLLN detection efficiency increased substantially over our analysis period, but OMI data coverage declined. However, the seasonal mean LNO_x production per flash does not seem to be affected by these changes.

Midlatitude and tropical (Central and West Africa, Central and South America, and Indonesia) analyses of LNO_x production efficiency are currently in progress and are being used to further examine the robustness of our methods. These studies are examining latitudinal variations, continental versus maritime variations, and the dependence of the production efficiency on flash rate. These analyses will be complemented by individual storm case studies that will help improve our analysis methods and aid in the refinement of an algorithm for global application. Future work includes analyses in relatively clear-sky conditions (CRF < 30%) downwind of storms using an alternative algorithm that better quantifies the background.

Acknowledgments

This research was funded under the NASA Aura Science Team. We thank Earth Networks, Inc., for use of the Earth Networks Total Lightning Network data and Megan Damon, who performed the GMI no-lightning simulations. We also thank Andy Weinheimer (NCAR), Tom Ryerson (NOAA), and Hans Schlager (DLR) for the NO_x data from the DC3 project. Daily gridded flash rate and OMI LNO_x data files for the Gulf of Mexico region for the June–August 2007 to 2011 period for the flash threshold value used in this analysis, along with an IDL program to read them, are available from http://croc.gsfc.nasa.gov/OMILNOx.

References

Allen, D. J., and K. E. Pickering (2002), Evaluation of lighting flash rate parameterizations for use in a global chemical transport model, *J. Geophys. Res.*, *107*(D23), 4711, doi:10.1029/2002JD002066.

Allen, D. J., K. E. Pickering, B. Duncan, and M. Damon (2010), Impact of lightning NO emissions on North American photochemistry as determined using the Global Modeling Initiative (GMI) model, *J. Geophys. Res.*, *115*, D22301, doi:10.1029/2010JD014062.

Allen, D. J., K. E. Pickering, R. W. Pinder, B. H. Henderson, K. W. Appel, and A. Prados (2012), Impact of lightning-NO on eastern United States photochemistry during the summer of 2006 as determined using the CMAQ model, *Atmos. Chem. Phys.*, *12*, 1737–1758, doi:10.5194/acp-12-1737-2012.

Allen, D. J., K. Pickering, A. Ring, A. Nag, and R. Holle (2014), Analysis of ground network lightning data relative to OTD/LIS to derive flash rates for use in determining lightning NO_x production from satellite observation, 5th International Lightning Meteorology Conference, Tucson, Ariz. [Available at http://www.vaisala.com/en/events/ildcilmc/Pages/ILDC-2014-archive.aspx.]

Barth, M. C., et al. (2015), The Deep Convective Clouds and Chemistry (DC3) field campaign, *Bull. Am. Meteorol. Soc.*, *96*, 1281–1309, doi:10.1175/BAMS-D-13-00290.1.

Beirle, S., U. Platt, M. Wenig, and T. Wagner (2004), NO_x production by lightning estimated with GOME, *Adv. Space Res.*, *34*(4), 793–797, doi:10.1016/j.asr.2003.07.069.

Beirle, S., et al. (2006), Estimating the NO_X produced by lightning from GOME and NLDN data: A case study in the Gulf of Mexico, *Atmos. Chem. Phys.*, *6*, 1075–1089.

Beirle, S., M. Salzmann, M. G. Lawrence, and T. Wagner (2009), Sensitivity of satellite observations for freshly produced lightning NO_X, *Atmos. Chem. Phys.*, *9*, 1077–1094.

Beirle, S., H. Huntrieser, and T. Wagner (2010), Direct satellite observation of lightning-produced NO_X, *Atmos. Chem. Phys.*, *10*, 10,965–10,986, doi:10.5194/acp-10-10965-2010.

Beirle, S., W. Koshak, R. Blakeslee, and T. Wagner (2014), Global patterns of lightning properties derived from OTD and LIS, *Nat. Hazards Earth Syst. Sci.*, *14*, 2715–2726, doi:10.5194/nhess-14-2715-2014.

Bertram, T. H., et al. (2007), Direct measurements of the convective recycling of the upper troposphere, *Science*, *315*, 816–820, doi:10.1126/science.1134548.

Boccippio, D. J., W. Koshak, R. Blakeslee, K. Driscoll, D. Mach, D. Buechler, W. Boeck, H. J. Christian, and S. J. Goodman (2000), The Optical Transient Detector (OTD): Instrument characteristics and cross-sensor validation, *J. Atmos. Oceanic Technol.*, *17*(4), 441–458.

Boccippio, D. J., W. J. Koshak, and R. J. Blakeslee (2002), Performance assessment of the Optical Transient Detector and Lightning Imaging Sensor. Part I: Predicted diurnal variability, *J. Atmos. Oceanic Technol.*, *19*, 1318–1332.

Boersma, K. F., H. J. Eskes, E. W. Meijer, and H. M. Kelder (2005), Estimates of lightning NO_x production from GOME satellite observations, *Atmos. Chem. Phys.*, *5*, 2311–2331.

Boersma, K. F., D. J. Jacob, H. J. Eskes, R. W. Pinder, J. Wang, and R. J. van der A (2008), Intercomparison of SCIAMACHY and OMI tropospheric NO_2 columns: Observing the diurnal evolution of chemistry and emissions from space, *J. Geophys. Res.*, *113*, D16S26, doi:10.1029/2007JD008816.

Boersma, K. F., et al. (2011), An improved tropospheric NO_2 column retrieval algorithm for the Ozone Monitoring Instrument, *Atmos. Meas. Tech.*, *4*, 1905–1928, doi:10.5194/amt-4-1905-1928.

Bond, D. W., S. Steiger, R. Zhang, X. Tie, and R. E. Orville (2002), The importance of NO_x production by lightning in the tropics, *Atmos. Env.*, *36*(9), 1509–1519, doi:10.1016/51352-2310(01)00553-2.

Bruning, E. C., and D. R. MacGorman (2013), Theory and observations of controls on lightning flash size spectra, *J. Atmos. Sci.*, *70*, 4012–4029.
Bucsela, E. J., et al. (2008), Comparison of tropospheric NO_2 from in situ aircraft measurements with near-real-time and standard product data from OMI, *J. Geophys. Res.*, *113*, D16S31, doi:10.1029/2007JD008838.
Bucsela, E. J., et al. (2010), Lightning-generated NO_X seen by the Ozone Monitoring Instrument during NASA's Tropical Composition, Cloud and Climate Coupling Experiment (TC^4), *J. Geophys. Res.*, *115*, D00J10, doi:10.1029/2009JD013118.
Bucsela, E. J., N. A. Krotkov, E. A. Celarier, L. N. Lamsal, E. H. Swartz, P. K. Bhartia, K. F. Boersma, J. P. Veefkind, J. F. Gleason, and K. E. Pickering (2013), A new stratospheric and tropospheric NO_2 retrieval algorithm for nadir-viewing satellite instruments: Applications to OMI, *Atmos. Meas. Tech.*, *6*, 2607–2626, doi:10.5194/amt-6-2607-2013.
Cecil, D. J., D. E. Buechler, and R. J. Blakeslee (2014), Gridded lightning climatology from TRMM-LIS and OTD: Dataset description, *Atmos. Res.*, doi:10.1016/j.atmosres.2012.06.028.
Choi, S., J. Joiner, Y. Choi, B. N. Duncan, A. Vasilkov, N. Krotkov, and E. Bucsela (2014), First estimates of global free-tropospheric NO_2 abundances derived using a cloud-slicing technique applied to satellite observations from the Aura Ozone Monitoring Instrument (OMI), *Atmos. Chem. Phys.*, *14*(19), 10,565–10,588.
Christian, H. J., et al. (1999), The Lightning Imaging Sensor, NASA Conf. Publ., pp. 746–749. [Available at http://thunder.msfc.nasa.gov/bookshelf/pubs/LIS_ICAE99_Print.pdf.]
Christian, H. J., et al. (2003), Global frequency and distribution of lightning as observed from space by the Optical Transient Detector, *J. Geophys. Res.*, *108*(D1), 4005, doi:10.1029/2002JD002347.
Chronis, T., W. Koshak, and E. McCaul (2016), Why do oceanic negative cloud-to-ground lightning exhibit larger peak current values?, *J. Geophys. Res. Atmos.*, *121*, 4049–4068, doi:10.1002/2015JD024129.
Cooper, O. R., et al. (2007), Evidence for a recurring eastern North America upper tropospheric ozone maximum during summer, *J. Geophys. Res.*, *112*, D23304, doi:10.1029/2007JD008710.
Cooper, O., et al. (2006), Large upper tropospheric ozone enhancements above midlatitude North America during summer: In situ evidence from the IONS and MOZAIC ozone measurement network, *J. Geophys. Res.*, *111*, D24S05, doi:10.1029/2006JD007306.
Cooray, V., R. Jayaratne, and K. L. Cummins (2014), On the peak amplitude of lightning return stroke currents striking the sea, *Atmos. Res.*, *149*, 372–376.
Cummings, K. A., T. L. Huntemann, K. E. Pickering, M. C. Barth, W. C. Skamarock, H. Holler, H. -D. Betz, A. Volz-Thomas, and H. Schlager (2013), Cloud-resolving chemistry simulation of a Hector thunderstorm, *Atmos. Chem. Phys.*, *13*, 2737–2777, doi:10.5194/acp-13-2757-2013.
Cummins, K. L., M. J. Murphy, E. A. Bardo, W. L. Hiscox, R. B. Pyle, and A. E. Pifer (1998), A combined TOA/MDF technology upgrade of the U.S. National Lightning Detection Network, *J. Geophys. Res.*, *103*(D8), 9035–9044, doi:10.1029/98JD00153.
DeCaria, A. J., K. E. Pickering, G. L. Stenchikov, J. R. Scala, J. L. Stith, J. E. Dye, B. A. Ridley, and P. Laroche (2000), A cloud-scale model study of lightning-generated NO_X in an individual thunderstorm during STERAO-A, *J. Geophys. Res.*, *105*(D9), 11,601–11,616, doi:10.1029/2000JD900033.
DeCaria, A. J., K. E. Pickering, G. L. Stenchikov, and L. E. Ott (2005), Lightning-generated NO_X and its impact on tropospheric ozone production: A three-dimensional modeling study of a Stratosphere-Troposphere Experiment: Radiation, Aerosols, and Ozone (STERAO-A) thunderstorm, *J. Geophys. Res.*, *110*, D14303, doi:10.1029/2004JD005556.
Dowden, R. J., J. B. Brundell, and C. J. Rodger (2002), VLF lightning location by time of group arrival (TOGA) at multiple sites, *J. Atmos. Sol. Terr. Phys.*, *64*, 817–830.
Duncan, B. N., S. E. Strahan, Y. Yoshida, S. D. Steenrod, and N. Livesey (2007), Model study of the cross-tropopause transport of biomass burning pollution, *Atmos. Chem. Phys.*, *7*, 3713–3736.
Gallardo, L., and V. Cooray (1996), Could cloud-to-cloud discharges be as effective as cloud-to-ground discharges in producing NO_X?, *Tellus*, *4b*, 641–651.
Hauglustaine, D., L. Emmons, M. Newchurch, G. Brasseur, T. Takao, K. Matsubara, J. Johnson, B. Ridley, J. Stith, and J. Dye (2001), On the role of lightning NO_x in the formation of tropospheric ozone plumes: A global model perspective, *J. Atmos. Chem.*, *38*, 277–294.
Huntrieser, H., U. Schumann, H. Schlager, H. Höller, A. Giez, H.-D. Betz, D. Brunner, C. Forster, O. Pinto Jr., and R. Calheiros (2008), Lightning activity in Brazilian thunderstorms during TROCCINOX: Implications for NO_X production, *Atmos. Chem. Phys.*, *8*, 921–953.
Huntrieser, H., et al. (2009), NO_X production by lightning in Hector: First airborne measurements during SCOUT-O3/ACTIVE, *Atmos. Chem. Phys.*, *9*, 8377–8412.
Huntrieser, H., H. Schlager, M. Lichtenstern, P. Stock, T. Hamburger, H. Höller, K. Schmidt, H.-D. Betz, A. Ulanovsky, and F. Ravengnani (2011), Mesoscale convective systems observed during AMMA and their impact on the NO_X and O_3 budget over West Africa, *Atmos. Chem. Phys.*, *11*, 2503–2536.
Hutchins, M. L., R. H. Holzworth, J. B. Brundell, and C. J. Rodger (2012), Relative detection efficiency of the World Wide Lightning Location Network, *Radio Sci.*, *47*, RS6005, doi:10.1029/2012RS005049.
Hutchins, M. L., R. H. Holzworth, K. S. Virts, J. M. Wallace, and S. Heckman (2013), Radiated VLF energy differences of land and oceanic lightning, *Geophys. Res. Lett.*, *40*, 2390–2394, doi:10.1002/grl.50406.
Intergovernmental Panel on Climate Change (2013), Climate Change 2013: The Physical Science Basis, in *Contribution of Working Group I to the Fifth Assessment Report of the Intergovernmental Panel on Climate Change*, edited by T. F. Stocker, et al., 1535 pp., Cambridge Univ. Press, Cambridge, U. K., and New York.
Jaeglé, L., D. J. Jacob, Y. Wang, A. J. Weinheimer, B. A. Ridley, T. L. Campos, G. W. Sachse, and D. E. Hagen (1998), Sources and chemistry of NO_X in the upper troposphere over the United States, *Geophys. Res. Lett.*, *25*(10), 1705–1708, doi:10.1029/97GL03591.
Koshak, W. (2014), Global Lightning Nitrogen Oxides Production, in *The Lightning Flash*, 2nd ed., edited by V. Cooray, chap. 19, 928 pp.
Koshak, W., H. Peterson, A. Biazar, M. Khan, and L. Wang (2014), The NASA Lightning Nitrogen Oxides Model (LNOM): Application to air quality modeling, *Atmos. Res.*, doi:10.1016/j.atmosres.2012.12.015.
Labrador, L. J., R. von Kuhlmann, and M. G. Lawrence (2004), Strong sensitivity of the global mean OH concentration and the tropospheric oxidizing efficiency to the source of NO_x from lightning, *Geophys. Res. Lett.*, *31*, L06102, doi:10.1029/2003GL019229.
Labrador, L. J., R. von Kuhlmann, and M. G. Lawrence (2005), The effects of lightning-produced NO_X and its vertical distribution on atmospheric chemistry: Sensitivity simulations with MATCH-MPIC, *Atmos. Chem. Phys.*, *5*, 1815–1834.
Lay, E. H., R. H. Holzworth, C. J. Rodger, J. N. Thomas, O. Pinto, and R. L. Dowden (2004), WWLL global lightning detection system: Regional validation study in Brazil, *Geophys. Res. Lett.*, *31*, L03102, doi:10.1029/2003GL018882.
Lay, E. H., C. J. Rodger, R. H. Holzworth, and R. L. Dowden (2005), Introduction to the World Wide Lightning Location Network (WWLLN), *Geophys. Res. Abstr.*, *7*, 02875.
Levelt, P. F., G. H. J. van den Oord, M. R. Dobber, A. Mälkki, H. Visser, J. de Vries, P. Stammes, J. O. V. Lundell, and H. Saari (2006a), The Ozone Monitoring Instrument, *IEEE Trans. Geosci. Remote Sens.*, *44*(5), 1093–1101.
Levelt, P. F., E. Hilsenrath, G. W. Leppelmeier, G. H. J. van den Oord, P. K. Bhartia, J. Tamminen, J. F. de Haan, and J. P. Veefkind (2006b), Science objectives of the Ozone Monitoring Instrument, *IEEE Trans. Geosci. Remote Sens.*, *44*(5), 1199–1208.

Liaskos, C. E., D. J. Allen, and K. E. Pickering (2015), Sensitivity of tropical tropospheric composition to lightning NO_x production as determined by replay simulations with GEOS-5, *J. Geophys. Res. Atmos.*, *120*, 8512–8534, doi:10.1002/2014JD022987.

Liu, C., and S. Heckman (2011), The application of total lightning detection and cell tracking for severe weather prediction, 91st American Meteorological Society Annual Meeting, Seattle.

Mach, D. M., H. J. Christian, R. J. Blakeslee, D. J. Boccippio, S. J. Goodman, and W. L. Boeck (2007), Performance assessment of the Optical Transient Detector and Lightning Imaging Sensor, *J. Geophys. Res.*, *112*, D09201, doi:10.1029/2006JD007787.

Marchenko, S., N. A. Krotkov, L. N. Lamsal, E. A. Celarier, W. H. Swartz, and E. J. Bucsela (2015), Revising the slant column density retrieval of nitrogen dioxide observed by the Ozone Monitoring Instrument, *J. Geophys. Res. Atmos.*, *120*, 5670–5692, doi:10.1002/2014JD022913.

Martin, R. V., B. Sauvage, I. Folkins, C. E. Sioris, C. Boone, P. Bernath, and J. Ziemke (2007), Space-based constraints on the production of nitric oxide by lightning, *J. Geophys. Res.*, *112*, D09309, doi:10.1029/2006JD007831.

Mecikalski, R. M., A. L. Bain, and L. D. Carey (2015), Radar and lightning observations of deep moist convection across northern Alabama during DC3 21 May 2012, *Mon. Weather Rev.*, *143*, 2774–2794, doi:10.1175/MWR-D-14-00250.1.

Olson, J. R., et al. (2005), An examination of photochemical theory based on INTEX-NA observations, *Eos Trans. AGU*, *86*(52), Fall Meet. Suppl., Abstract A51C-0063.

Ott, L. E., K. E. Pickering, G. L. Stenchikov, H. Huntrieser, and U. Schumann (2007), Effects of lightning NO_X production during the 21 July European Lightning Nitrogen Oxides Project storm studied with a three-dimensional cloud-scale chemical transport model, *J. Geophys. Res.*, *112*, D05307, doi:10.1029/2006JD007365.

Ott, L. E., K. E. Pickering, G. L. Stenchikov, D. J. Allen, A. J. DeCaria, B. Ridley, R.-F. Lin, S. Lang, and W.-K. Tao (2010), Production of lightning NO_x and its vertical distribution calculated from three-dimensional cloud-scale chemical transport model simulations, *J. Geophys. Res.*, *115*, D04301, doi:10.1029/2009JD011880.

Pickering, K. E., A. M. Thompson, R. R. Dickerson, W. T. Luke, D. P. McNamara, J. P. Greenberg, and P. R. Zimmerman (1990), Model calculations of tropospheric ozone production potential following observed convective events, *J. Geophys. Res.*, *95*(D9), 14,049–14,062, doi:10.1029/JD095iD09p14049.

Pickering, K. E., A. M. Thompson, W.-K. Tao, and T. L. Kucsera (1993), Upper tropospheric ozone production following mesoscale convection during STEP/EMEX, *J. Geophys. Res.*, *98*(D5), 8,737–8,749, doi:10.1029/93JD00875.

Pickering, K. E., et al. (1996), Convective transport of biomass burning emissions over Brazil during TRACE A, *J. Geophys. Res.*, *101*(D19), 23,993–24,012, doi:10.1029/96JD00346.

Pickering, K. E., Y. Wang, W.-K. Tao, C. Price, and J.-F. Müller (1998), Vertical distributions of lightning NO_X for use in regional and global chemical transport models, *J. Geophys. Res.*, *103*(D23), 31,203–31,216, doi:10.1029/98JD02651.

Price, C., J. Penner, and M. Prather (1997), NO_X from lightning: 2. Constraints from the global atmospheric electric circuit, *J. Geophys. Res.*, *102*(D5), 5,943–5,951, doi:10.1029/96JD02551.

Ridley, B., et al. (2004), Florida thunderstorms: A faucet of reactive nitrogen to the upper troposphere, *J. Geophys. Res.*, *109*, D17305, doi:10.1029/2004JD004769.

Rienecker, M. M., et al. (2011), MERRA: NASA's Modern-Era Retrospective Analysis for Research and Applications, *J. Clim.*, *24*(14), 3624–3648, doi:10.1175/JCLI-D-00015.1.

Rodger, C. J., J. B. Brundell, R. L. Dowden, and N. R. Thomson (2004), Location accuracy of long distance VLF lightning location network, *Ann. Geophys.*, *22*, 747–758.

Rodger, C. J., J. B. Brundell, and R. L. Dowden (2005), Location accuracy of VLF World-Wide Lightning Location (WWLL) network: Post-algorithm upgrade, *Ann. Geophys.*, *23*, 277–290.

Rodger, C. J., J. B. Brundell, R. H. Holzworth, and E. H. Lay (2009), Growing detection efficiency of the World Wide Lightning Location Network, *AIP Conf. Proc.*, *1118*, doi:10.1063/1.3137706.

Rudlosky, S. D., and D. T. Shea (2013), Evaluating WWLLN performance relative to TRMM/LIS, *Geophys. Res. Lett.*, *40*, 1–5, doi:10.1002/grl.50428.

Schumann, U., and H. Huntrieser (2007), The global lightning-induced nitrogen oxides source, *Atmos. Chem. Phys.*, *7*, 3823–3907.

Seinfeld, J. H., and S. N. Pandis (2006), *Atmospheric Chemistry and Physics: From Air Pollution to Climate Change*, Wiley-Interscience, New York.

Strode, S. A., J. M. Rodriguez, J. A. Logan, O. R. Cooper, J. C. Witte, L. N. Lamsal, M. Damon, B. Van Aartsen, S. D. Steenrod, and S. E. Strahan (2015), Trends and variability in surface ozone over the United States, *J. Geophys. Res. Atmos.*, *120*, 9020–9042, doi:10.1002/2014JD022784.

Tie, X., R. Zhang, G. Brasseur, and W. Lei (2002), Global NO_X production by lightning, *J. Atmos. Chem.*, *43*, 61–74.

Tost, H., P. Jockel, and J. Lelieveld (2007), Lightning and convection parameterizations—Uncertainties in global modeling, *Atmos. Chem. Phys.*, *7*(17), 4553–4568.

van der Werf, G. R., J. T. Randerson, L. Giglio, G. J. Collatz, M. Mu, P. S. Kasibhatla, D. C. Morton, R. S. DeFries, Y. Jim, and T. T. van Leeuwen (2010), Global fire emissions and the contribution of deforestation, savanna, forest, agricultural, and peat fires (1997–2009), *Atmos. Chem. Phys.*, *10*, 11,707–11,735.

van Donkelaar, A., et al. (2008), Analysis of aircraft and satellite measurements from the Intercontinental Chemical Transport Experiment (INTEX-B) to quantify long-range transport of East Asian sulfur to Canada, *Atmos. Chem. Phys.*, *8*, 2999–3014.

Vasilkov, A., J. Joiner, R. Spurr, P. K. Bhartia, P. Levelt, and G. Stephens (2008), Evaluation of the OMI cloud pressures derived from rotational Raman scattering by comparisons with other satellite data and radiative transfer simulations, *J. Geophys. Res.*, *113*, D15S19, doi:10.1029/2007JD008689.

Virts, K. S., J. M. Wallace, M. L. Hutchins, and R. H. Holzworth (2013), Highlights of a new ground-based, hourly global lightning climatology, *Bull. Am. Meteorol. Soc.*, *94*, 1381–1392.

Wang, Y., A. W. DeSilva, G. C. Goldenbaum, and R. R. Dickerson (1998), Nitric oxide production by simulated lightning: Dependence on current, energy, and pressure, *J. Geophys. Res.*, *103*(D15), 19,149–19,159, doi:10.1029/98JD01356.

Yevich, R., and J. A. Logan (2003), An assessment of biofuel use and burning of agricultural waste in the developing world, *Global Biogeochem. Cycles*, *17*(4), 1095, doi:10.1029/2002GB001952.

Zeldovich, Y. B., P. Y. Sadovnikov, and D. A. Frank-Kamenetskii (1947), *Oxidation of Nitrogen in Combustion*, translation by M. Shelef, Academy of Sciences of USSR, Institute of Chemical Physics, Moscow-Leningrad.

Zhang, Q., et al. (2009), Asian emissions in 2006 for the NASA INTEX-B mission, *Atmos. Chem. Phys.*, *9*, 5131–5153.

Zhang, R., X. Tie, and D. W. Bond (2003), Impacts of anthropogenic and natural NO_X sources over the U.S. on tropospheric chemistry, *Proc. Natl. Acad. Sci. U.S.A.*, *100*(4), 1505–1509.

Ziemke, J. R., S. Chandra, B. N. Duncan, L. Froidevaux, P. K. Bhartia, P. F. Levelt, and J. W. Waters (2006), Tropospheric ozone determined from Aura OMI and MLS: Evaluation of measurements and comparison with the Global Modeling Initiative's Chemical Transport Model, *J. Geophys. Res.*, *111*, D19303, doi:10.1029/2006JD007089.